Chapter

Ti_3C_2 MXene-Based Nanobiosensors for Detection of Cancer Biomarkers

Lenka Lorencova, Kishor Kumar Sadasivuni, Peter Kasak and Jan Tkac

Abstract

This chapter provides information about basic properties of MXenes (2D nanomaterials) that are attractive for a design of various types of nanobiosensors. The second part of the chapter discusses MXene synthesis and various protocols for modification of MXene making it a suitable matrix for immobilization of bioreceptors such as antibodies, DNA aptamers or DNA molecules. The final part of the chapter summarizes examples of MXene-based nanobiosensors developed using optical, electrochemical and nanomechanical transducing schemes. Operational characteristics of such devices such as sensitivity, limit of detection, assay time, assay reproducibility and potential for multiplexing are provided. In particular MXene-based nanobiosensors for detection of a number of cancer biomarkers are shown here.

Keywords: MXene, nanomaterials, biosensors, cancer, biomarkers

1. Introduction

1.1 MXenes: their precursors, characterization, unique properties and applications

Nanomaterials of the 2D kind are in the research spotlight due to their superior properties like ultrathin structure and intriguing physico-chemical properties [1–3]. Graphene has made researchers believing in extracting single layer transition metal dichalcogenides, which in turn has led to extensive research dedicated towards 2D nanomaterials [4, 5]. Since their inception, 2D nanomaterials have been characterized to have exceptional electronic, mechanical, and optical properties. These outstanding characteristics have driven research to use them in almost all fields of materials science and nanotechnology [6–8]. Rather recently in 2011 and 2012, Gogotsi, Barsoum, and colleagues have successfully prepared a new kind of 2D nanomaterial - MXenes, composed of a large group of transition metal carbides and carbonitrides [9–13]. These 2D nanomaterials are found to possess many striking properties and boost attraction in applications such as energy storage [14–16], electromagnetic shielding [17, 18], water treatment [19, 20], disease treatment [21] and (bio)sensing [22, 23], MXenes are made up of atomic layers of different materials like transition metal carbides, nitrides, or carbonitrides. All MAX phases consist of two-dimensional slabs of close-packed alternating layers of *M* and *A*, where *M* is a transition metal, *A* is an A-group element and *X* is C and/or N [23].

The selective chemical etching of "A" in "MAX" phases have led to successful synthesis of MXenes. MAX phases are found to have elusive properties like stiff elasticity, good thermal and electrical conductivity, as well as relatively low thermal expansion coefficients and resistance towards chemical attack. There is a general formula for MXene synthesis where, "MAX" phases have a formula of $M_{n+1}AX_n$, with "M" meaning early d-transition metal, "A" representing the main group sp-element, and "X" indicates C and/or N [24]. Hence, with this analogy, more than 70 different kinds of MXenes with different M and X are theoretically possible to synthesize. Out of these theoretical MXene types, 20 different combinations of MXenes have been synthesized successfully [25]. MXenes can conduct heat and electricity like metals and are strong and brittle like ceramics with high surface area. Exfoliated MXene exhibits higher pseudocapacitance than most capacitive materials [26]. Additionally, the MXene-have properties like a clay. Furthermore, Ca^{2+}, Mg^{2+} and Al^{3+} ions (intercalated polyvalent cations) have all shown a huge storage power capacity [27–29]. It needs to be stressed out that energy storage capacity, high conductivity, photochemical properties, modulated surface chemistry and tunable composition make MXene and their derivatives very perspective to (bio)sensing applications.

2D MXenes are candidates for energy storage [30] (Li-ion batteries, supercapacitors) and electromagnetic interference shielding applications [31–35] and in the form of composites become ever more useful for sensing as *e.g.* gas sensing devices [36, 37], pressure sensor [38, 39] and sensors for various analytes [40–43]. Number of other biomedical applications (such as biosensor, biological imaging, photothermal therapy, drug delivery, theranostic nanoplatforms and antibacterial agents) have become a challenge for MXenes [44]. The antibacterial properties making them potentially appealing for nanomedicine were proved for ($Ti_3C_2T_x$) MXene quantum dots [45], MXene-hybridized silane film [46], Cu_2O/MXene [47] and MXene-gold nanoclusters [48] *etc*. The multifunctional MXenes have attracted attention in biosensing [49, 50] with the aim at the ultrasensitive determination of cancer diseases related biomarkers. Examples include biosensors based on Ti_3C_2 MXenes-Au NPs hybrids, delaminated $Ti_3C_2T_x$ MXene@AuNPs, nanohybrid of $Ti_3C_2T_x$ MXene and phosphomolybdic acid (PMo_{12}) embedded with polypyrrole, MXene-TiO_2/$BiVO_4$ hybrid and AuNPs/Ti_3C_2 MXene three-dimensional nanocomposite for detection of carcinoembryonic antigen [51], prostate specific antigen [52], osteopontin [53], CD44 [54] and microRNA-155 [55], respectively.

2. MXene synthesis

Generally, top-down selective etching process is used for the synthesis of MXenes [56]. Strong etching solutions containing a fluoride ion (F^-) such as hydrofluoric acid (HF), ammonium difluoride (NH_4HF_2), and a mixture of hydrochloric acid (HCl) and lithium fluoride (LiF) are used for production of MXene in such processes [57]. Since typically, the etching process results in replacement of the M-A bond by M-O, M-OH, M-H, and M-F bonds on the surface of MXenes, the structure of MXenes can be expressed as $M_{n+1}X_nT_x$ or $M_{n+1}X_n$ (M and X are in same form as the MAX phase and T is =O, -OH, -H, or -F) [58, 59].

A single and/or few layers of MXene can be synthetized by exfoliation or delamination of a multilayer structure of a MAX phase. The composition and electrochemical properties of MXene strongly depend on the conditions used during etching procedure [60]. As an example, application of LiF/HCl as etchant led to production of MXene with interlayers intercalated with Li^+ ions. Exfoliation can be

done by a simple shaking or by sonication and prolonged sonication time results in production of MXene with small size of nanosheets and high density of defects [61]. An alternative to use of highly corrosive and harmful HF is to employ small organic molecules or ions such as urea [62], dimethyl sulphoxide (DMSO) [12] (only for $Ti_3C_2T_x$ MXene) or isopropylamine as etchants [63]. MAX phase containing Si can be also exfoliated using tetrabutylammonium hydroxide (TBAOH) and tetramethylammonium hydroxide (TMAOH) [64].

3. MXene characterization

Since introduction of nanolayered and machinable MXenes in 2011 by Gogotsi and co-workers through wet-etching process with HF to obtain multilayered flakes of $Ti_3C_2T_x$ [13], few improvements in MXene synthesis and MXene-nanocomposite preparation resulted in various elemental composition and surface functionality [65]. In last few years the single layers of MXene were isolated adding salts or organic solvents (NH_4HF_2, tetrabuthylammonium hydroxide, isopropylamine) during synthesis process and resulted in delaminated MXene layers. The significant breakthrough for MXene synthesis named as "clay method" in 2014 was based on *in situ* formation of HF (LiF/HCl). The lattice *c* parameter increased to a value of ≈40 Å by applying LiF-HCl as an etchant to produce $Ti_3C_2T_x$ instead of HF etchant with a lattice *c* parameter of 20 Å [60]. The battery of techniques were employed to observe variations in the composition of $Ti_3C_2T_x$ MXene produced either by HF or LiF-HCl method including nuclear magnetic resonance (^1H, ^{13}C and ^{19}F NMR), scanning electron microscopy (SEM), X-ray diffraction method (XRD), energy-dispersive X-ray spectroscopy (EDS) techniques [59]. The most suitable combination presented utilization of LiF/HCl as an etchant with minimally intensive layer delamination "MILD" method instead of sonication to produce huge MXene flakes with minimum of defects [66]. $Ti_3C_2T_x$ MXene has become an attractive subject of interest due its high capacitance (∼1500 F cm^{-3}) in supercapacitors and an excellent high metallic conductivity (∼15,000 S cm^{-1}). On the other hand there is still demand to improve stability of MXene flakes with a poor resistance in aerated aqueous suspensions resulting in oxidized form with loss of its activity for potential applications [67]. The optimization of etching process is cardinal to access single- to few-layer Ti_3C_2 MXene flakes. SEM technique providing information about flake size and distribution revealed formation of aggregates on the surface varying in size i.e. having few μm in size or with size larger than 10 μm in a lateral dimension. It was found out by atomic force microscopy (AFM), that thickness of single MXene monolayer was (1.1 ± 0.1) nm for $Ti_3C_2T_x$ [68]. Platinum nanoparticles with average diameter of 3 nm were homogeneously distributed on the MXene sheets surface, that was found out by transmission electron microscopy (TEM) [69]. MXene and oxidized MXene were analyzed and differentiated by applying Raman spectroscopy method providing more detailed information about the characteristic vibrational bands and the dependence thickness of Ti_3C_2Tx layers on Raman signal enhancement [68–71].

The electrochemical behavior employing methods like cyclic voltammetry (CV), chronoamperometry (CA), differential pulse voltammetry (DPV) and electrochemical impedance spectroscopy (EIS) revealed significant findings related to the electrochemical activity of MXene. The electrochemical investigation of $Ti_3C_2T_x$ MXene to detect significant analytes (O_2, H_2O_2 and NADH) was performed by applying cyclic voltammetry and chronoamperometry techniques, whereas $Ti_3C_2T_X$ demonstrated electrocatalytic activity towards H_2O_2 reduction with LOD at nanomolar level [68]. Unfortunately, formation of TiO_2 layer or domains with

subsequent TiO_2 dissolution caused by F^- ions was observed during oxidation process at anodic potential window in a plain phosphate buffer electrolyte pH 7.0 leading to the decrease in electrochemical activity of $Ti_3C_2T_x$ MXene.

The improvement of stability and redox behavior was achieved by further modification of MXene with nanoparticles of platinum ($Ti_3C_2T_x$/Pt) [69, 72]. The electrocatalytically active sensor based on $Ti_3C_2T_x$/Pt nanocomposite successfully determined H_2O_2 by CA, and moreover small organic molecules (acetaminophen, dopamine, ascorbic acid, uric acid) were selectively determined by DPV [72].

In addition electrochemical study confirmed significant differences in a negative charge density on the MXene surface as well electrocatalytic activity depending on the etchant (HF, LiF/HCl) used during MXene synthesis with preference towards utilization of LiF/HCl [60].

Aryldiazonium salts were utilized in modification of $Ti_3C_2T_x$ MXene either spontaneously by free electrons or electrochemically. Electrochemical modification of $Ti_3C_2T_x$ MXene by aryldiazonium-based grafting with derivatives bearing a SB- or CB- betaine pendant moiety was performed by cyclic voltammetry in a potential window from 0 V to −1 V with a sweep rate of 0.25 V s^{-1} and 48 cycles. The electrochemical grafting resulted in denser CB or SB layer on MXene interface, lower interfacial resistance and an electrochemically active surface area for SB layer in comparison to CB layer [73].

In the following years the exponential increase in the number of affinity-based MXene biosensors can be expected, though it is necessary to develop advanced strategies for modification of MXene interfaces with an effort to eliminate non-specific binding of proteins, bring in anti-fouling behavior and immobilize target biomolecules. Electrochemical methods can be employed as a useful tools for interfacial patterning, characterization of MXene-based biosensors and furthermore ultrasensitive detection of cancer related biomarkers [23].

4. MXene functionalization

4.1 Covalent modification of Ti_3C_2 MXenes with biomolecules

Functionalization and various methods for synthesis of MXenes can result in production of the nanomaterial with a diverse range of properties. This is why, it is very important to describe synthesis of MXenes in full details. Another point to focus on is to properly describe delamination conditions since the flake size and density of defects governs MXene's surface properties and stability. It is important to know the molecular structure of MXenes in order to decide the best application of such nanomaterial for catalysis, (bio)sensing or for chemical adsorption of various compounds.

Due to presence of -OH groups on surface, functionalization of MXene employing silylation reagents was developed by a simple reaction with triethoxysilane derivatives [74–76]. Such modification led to production of nanosheets of Ti_3C_2-MXene uniformly patterned by aminosilane moieties allowing NHS/EDC-based amine coupling for covalent immobilization of bioreceptors such as anti- carcinoembryonic antigen (CEA) antibodies [77].

Another viable surface modification of MXenes can be done by applying zwitterions. It was observed that spontaneous grafting of sulfobetaine (SB) and carboxybetaine (CB) derivatives onto $Ti_3C_2T_x$ MXene is feasible [73]. The approach is similar to spontaneous grafting of diazonium salt modified zwitterions to gold nanoshell modified particles by consuming surface plasmons (free electron cloud) present within Au nanoshells [78]. Even though spontaneous grafting of diazonium

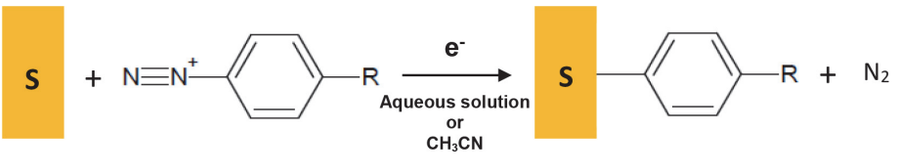

Figure 1.
Electrochemically triggered grafting of diazonium salt-containing compounds to conductive surfaces. Electrochemical reduction of diazonium salt-containing compounds is feasible via freely available clouds of electrons (plasmons) present in metallic nanoparticles, but also in MXene.

salt modified zwitterions to MXene was feasible, electrochemically triggered grafting of diazonium salts bearing zwitterionic pendants was more effective (**Figure 1**) [73]. Electrochemical characterization tools confirmed a much quicker spontaneous SB grafting compared to spontaneous CB grafting. Zwitterionic modification is considered as a benchmark to design antibiofouling interfaces with such modification offering to reduce dramatically non-specific protein binding compared to an unmodified MXene interface [73]. It is worth mentioning that grafting of a mixed layer composed of CB and SB can be applied to tune density of carboxylic groups and by amine coupling chemistry it is possible to finely tune density of immobilized bioreceptors for effective and efficient recognition of an analyte *via* affinity interactions [79]. Diazonium salts can be utilized in order to achieve stable modification of all surfaces (radical reaction providing most often disordered oligomers ("multilayers")) [80].

> *Diazonium salts can be easily synthetized from aromatic amines that are commercially available. Modification can be performed by applying different grafting methods like electrochemistry, spontaneous reduction, by reducing surfaces and reagents, photochemistry etc.*

Besides application of APTES there are other strategies for modification of MXene such as self-initiated photo-grafting and photopolymerization not requiring an anchor layer, self-assembled monolayer (SAM) and initiator, applying a nature polymer, soy phospholipid (SP) improving permeability, stable cycling, and retention and PEGylation of MXene improving the water dispersibility of MXene by electrostatic adsorption [81].

Recently, a novel MXene modification approach was developed by substitution or elimination reactions in molten inorganic salts. Such modification allowed to synthetize MXenes containing = O, -NH, =S, -Cl, -Se, -Br, and -Te surface terminations [82].

4.2 Preparation of hybrid nanoparticles based on MXene

The hydrothermal method run in a Teflon-lined stainless steel autoclave (150°C, 5 h; aqueous solution of vitamin C and Fe^{3+} salt) allowed preparation of composite of MXene with small magnetic Fe_3O_4 nanoparticles with an average size of ~4.9 nm (TiO_2/$Ti_3C_2T_x$/Fe_3O_4). These hybrid magnetic nanoparticles show a great promise for selective enrichment of various biomolecules/antigens based on affinity interactions [83].

Other promising nanocomposite option is represented by MXene sheets combined with metallic NPs [84–87], which can be further effectively modified by crosslinkers due to their high affinity towards MXene or by other biomolecules for final detection of target molecules/biomarkers. MXene/metallic nanoparticles (NPs) based nanocomposites can be prepared by spontaneous reduction of salts of precious metals or by applying an external reducing agent such as $NaBH_4$. A simple spontaneous reduction of metallic salts to form Ag, Au, and Pd nanoparticles onto

the $Ti_3C_2T_x$ MXene sheets was applied for formation of particles exhibiting surface–enhanced Raman spectroscopy (SERS) phenomenon [85]. Moreover, an AuNP/MXene composite boosts sensitivity of detection of oncomarker such as microRNA [88]. Similarly, the composite consisting of $Ti_3C_2T_x$ MXene and PtNPs was prepared by means of *in-situ* reduction of Pt precursor (spontaneously or by external reducing agents) on MXene surface. Composite was used for electrochemical catalysis [69] and sensing of important small bioactive compounds [72]. The negatively charged acetylcholinesterase (AChE) was electrostatically deposited on the hybrid nanocomposite of MXene/AgNPs/chitosan from a mixture of the enzyme and chitosan onto MXene/AuNPs for detection of organophosphate pesticide [86].

Graphite oxide as another 2D material was used to form composite together with MXene and such a composite led to a stable and efficient electrochemical detection of H_2O_2 and maintained hemoglobin biological activity even after ink jet printing applied for a sensor-based application [89].

4.3 Electrostatic and other interactions

MXene surface can be patterned *via* electrostatic interactions between MXene and chitosan making a nanocomposite from a negatively charged $Ti_3C_2T_x$ MXene and positively charged biopolymer. Chitosan due to beneficial properties i.e. biocompatibility, nontoxicity and film-forming ability was successfully applied in numerous studies for preparation of MXene/chitosan bionanocomposites or hybrid MXene/chitosan-based nanoparticles. Such a bionanocomposite was used for attachment of an enzyme sarcosine oxidase for detection of sarcosine as a potential prostate cancer biomarker. The biosensor could detect the analyte from LOD of 18 nM up to 7.8 μM. The device responded to the analyte in an extremely short time of 2 s and the analyte was detected in a complex sample with recovery index of 102.6% (**Figure 2**) [90]. Glutaraldehyde was not needed for immobilization of the enzyme [90]. Such approach with glutaraldehyde was also used in other studies [91, 92]. In addition Nafion was proved to be an effective "adhesive" to deposit MXene onto the surface, e.g. for a final electrostatic immobilization of glucose oxidase (GOx) [84], to deposit MXene with adsorbed hemoglobin [93, 94], MXene/$Mn_3(PO_4)_2$ hybrid particles [95] or MXene/TiO_2 mixed with hemoglobin on GCE [96].

DNA aptamer activated through EDC/NHS chemistry was covalently immobilized onto MXene electrostatically modified with polyethyleneimine (PEI) [97].

Zheng *et al.* [98] described *in situ* adsorption of DNA on MXene surface through aromatic hydrophobic bases and in further step modified Ti_3C_2/DNA interface was patterned by PdNPs and PtNPs deposited using $NaBH_4$ as a reducing agent to obtain Ti_3C_2/DNA/Pd/Pt nanocomposite.

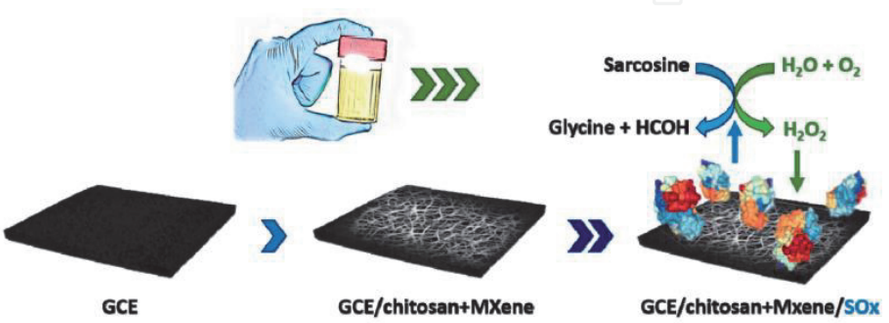

Figure 2.
A graphical presentation of a glassy carbon electrode (GCE) modified using a MXene/chitosan nanocomposite as a support for sarcosine oxidase (SOx) immobilization and indirect sarcosine detection in urine, based on hydrogen peroxide electrochemical reduction. SOx structure is adapted from the protein data Bank (code 1EL5). Figure taken from Ref. [90].

Any conductive interface can be patterned by MXene by a simple casting of a MXene dispersion on untreated electrodes with formation of MXene layer after drying [73]. Alternatively, the electrodes can be pretreated in order to make them more adhesive for formation of MXene layer. To make surface of screen-printed electrodes (SPEs) hydrophilic for subsequent deposition of MXene, SPEs were electrochemically activated in 0.1 M NaOH by CV in a potential range from −0.6 V to 1.3 V [50]. SPEs patterned with delaminated MXene suspension as signal enhancer were applied for quantifying acetaminophen (ACOP) and isoniazid (INZ) in blood serum samples [99]. The presence of abundant highly active surface sites due to functional groups (=O, -F and -OH) offers additional opportunity for MXene to interact with various positively charged functional groups of molecules.

Besides electrostatic modification of MXene by a modifier applied as glue for subsequent attachment of bioreceptors, electrostatic interactions could be applied also to modify MXene by redox molecules. Methylene blue as a redox probe due to its positive charge can be electrostatically deposited on MXene layer with a final immobilization of the enzyme urease on the surface using glutaraldehyde [50]. Moreover electrostatic interaction was utilized for deposition of positively (CTA^+) charged cetyltrimethylammonium chloride (CTAC) on the negatively (OH^-) charged Nb_2C nanosheets resulting in CTAC-anchored Nb_2C nanosheets and subsequently *in situ* formation of mesoporous silica layer (a pore size of 2.9 nm) by co-deposition of CTAB and tetraethyl orthosilicate (TEOS) in the next step [100].

Rich surface chemistry of MXenes can be also applied for interaction with a number of molecules. High applicability of exfoliated MXene (e-MXene) has been investigated as a matrix due to its high laser energy absorption, electrical conductivity and photothermal conversion for laser desorption/ionization time-of-flight mass spectrometry (LDI-MS) analysis of various analytes (saccharides - glucose, sorbitol, sucrose, and mannitol, amino acids - Arg, Phe, His, and Pro, peptide - leu-enkephalin and antibiotics - sulfamerazine and norfloxacin, benzylpyridinium salt (BP), environmental pollutants). Before LDI-MS measurement 1 μL of each small molecule solution was spotted on a target plate, mixed with 1 μL of e-MXene suspension and dried under ambient condition. The e-MXenes exhibiting a high resolution and salt-tolerance demonstrated a strong potential for the development of an efficient analytical platform based on LDI-MS analysis [101]. In addition, Ti_3C_2 MXene assisted LDI-LIFT-TOF/TOF was utilized for differentiation and relative quantitative analysis of three types of glycan isomers resulting in higher sensitivity, better homogeneity and stable relative peak intensity for glycan analysis. Moreover nine disaccharides, two trisaccharides, three heptasaccharides and ten natural product extractions were resolved by applying MXene with LDI-LIFT-MS/MS. The enhanced sensitivity and background-free nature of the fragment profile obtained by LDI-LIFT-TOF/TOF opens up a new realm for nanomaterial assisted glycan structural analysis and/or enrichment either through MXenes themselves or in combination with other functionalized magnetic nanoparticles [102].

Glycans are biomolecules, both simple and complex carbohydrates playing important roles in molecular recognition, protein conformation, cell proliferation and differentiation. The analysis of glycans and their structure has gained considerable attention because of their close relationship with disease occurrence and progression. Major types of glycans include N-linked glycans attached to the nitrogen atom in the asparagine side chain within a consensus amino acid sequence Asn-X-Ser/Thr (X should not be proline), and O-linked glycans attached to the oxygen atom of several amino acid residues including serine and threonine. Other types of glycans include glycosaminoglycans usually found attached to the proteins (proteoglycans) and also lipid chains as in glycolipids. MXenes can play an important role in the hydrogen-bonding interactions with glycans and in metal ions (Na^+/K^+) enrichment and transfer leading to improvement of the ionization efficiency of glycans.

5. Advanced 2D MXenes-based nanobiosensors as ultrasensitive detection tools

The link between progressive detection and daily/routine tests is fostered by (bio)sensing platforms employing nanomaterials/nanostructures with outstanding electronic, electrocatalytic, magnetic, mechanical, and optical properties. Novel multifunctional nanometer-sized structures combine advantageous large surface-to-volume ratio, controlled morphology and structure that would allow immobilizing bioreceptors with preserved biocompatibility, biostability and biodistribution [103]. Compared to other 2D materials (graphene, graphitic carbon nitride, MoS_2), MXenes nanomaterials carry a unique combination of excellent electrical conductivity, complete metal atomic layers, ease of functionalization, high stability, hydrophilicity, large surface area, ultrathin 2D sheet-like morphology, excellent mechanical properties and good bio-compatibility [49, 77].

Bioreceptor‘s intrinsic characteristics including its affinity towards the analyte, structural stability during biosensor’s operation and a methodology deployed for bioreceptor immobilization onto the transducing surface can significantly affect sensitivity, selectivity and robustness (reproducibility, stability *etc*.) of a biosensor. The biorecognition element is usually grafted onto a surface, *i.e*., in the close vicinity of the transducer. Additional specifications, which need to be optimized for advanced biosensing performance, are the accessibility of the analyte to the biorecognition site of the bioreceptor, the distance between the bioreceptor and the transducer (surface) and bioreceptor’s interfacial density.

Both enhanced biocompatibility and increase of the transducing surface area of the (bio)sensors related to enhanced catalytic activity drive a design of 2D MXene nanomaterial-based biosensors utilizing aptamers, antibodies, enzymes and protein molecules [23, 60, 68]. Ultrathin 2D sheet-like morphology with potential for high density incorporation of a number of functional groups as well as excellent ion intercalation behavior also show up as promising features for (bio)sensing applications [104]. On the other hand the implementation of MXenes as next-generation detection devices will require a substantial improvement of the stability of MXenes towards oxidation.

“Detect-to-protect” biosensors are compact analytical devices converting the biochemical reaction into an analytical and measureable signal. Due to their high specificity which is directly dependent on the receptor used (biomolecules or synthetic compounds), their sensitivity, compact size and simple operation, biosensors are the tool of choice for detection of chemical and biological components. Principally, biosensors are formed by two components, a biorecognition part consisting of a biological or synthetic receptor (enzymes, antibodies, nucleic acids, organelles, plant and animal tissue, whole organism, or organs) that utilizes a specific biochemical or chemical reaction mechanism with an analyte and a transducer where the interaction between a bioreceptor and an analyte is transformed into a measurable signal. There are two major obstacles in biosensor development; incorporation/immobilization of (bio)receptors in suitable matrix and monitoring/quantifying the interactions between the analytes and these receptors [105].

In order to allow for a rapid screening of analytes/antigens from human samples a real-time analysis is the preferred approach. The corresponding biosensor should be cheap, small, portable and user-friendly.

The key part of a biosensor is the transducer, which screens a physical change accompanying the bioaffinity reaction (*amperometric biosensors, calorimetric biosensors, optical biosensors, piezo-electric biosensors, potentiometric biosensors*).

A typical biosensor consists of:
1. a bioreceptor that specifically bind to the analyte;
2. an interface architecture where a specific biological event takes place and gives rise to a signal screened by such an interface;
3. a transducer element converting a biorecognition event into a measurable signal;
4. a computer software able to further process and store measured signal;
5. an interface to the human operator.

The morphology of ultrathin 2D Ti_3C_2 MXene single or few layered nanosheets with high density of functional groups offers improved biomolecule loading and rapid access to the analyte. The covalent immobilization of biorecognition elements (DNAs, enzymes, proteins, *etc.*) leads not only to improved uniformity and accessibility of immobilized bioreceptors, but also to higher density of bound bioreceptors, all resulting in an enhanced biosensor performance.

Jastrzębska *et al*. observed that 2D Ti_3C_2 MXene superficially oxidized into titanium (III) oxide i.e., Ti_2O_3 by sonication of MXene flakes followed by a mild thermal oxidation in water at 60°C for 24 h resulted in "fine-tuning" of the toxicity of the flakes to cancerous cell lines. The authors found out, that thermally oxidized samples showed the highest cytotoxic effect, moreover they were selectively toxic towards all cancerous cell lines with increasing concentration of nanomaterial up to 375 mg L^{-1} [106].

5.1 State-of-the-art approaches of MXenes-based nanobiosensors for cancer biomarkers detection

Cancer is one of the deadliest diseases worldwide, and acquiring cancer-specific data by quantitative analysis of cancer-associated biomarkers is crucial to monitor cancer progression and for the early treatment [107]. As reported by the World Health Organization, the year of 2030 should be marked by approximately 12 million cancer related deaths, making cancer a major public health problem and one of the most prominent death-causing factors worldwide. The number of new cases of cancer (cancer incidence) is presently around 439 *per* 100,000 *per* capita *per* year [108]. Early-stage diagnostics of various types of cancer diseases is important since it offers opportunities to extend life expectation of patients. Tumor markers exist in tumor cells themselves or are secreted by tumor cells. In either case the presence of these tumor markers above a set threshold may suggest the existence and/or growth of a tumor. The phrase "tumor marker" is often transposed for the term "biomarker" [109] and *vice versa*. Biomarkers can be applied as an early diagnostic tool, to monitor disease progression, as a prognostic tool and as means for prediction and monitoring of clinical response to an intervention.

According to the National Institute of Health, a biological marker (biomarker): is a characteristic that is objectively measured and evaluated as an indicator of normal biological processes, pathogenic processes, or pharmacologic responses to a therapeutic intervention.

A tumor/cancer marker is a substance produced by a tumor or by the host in response to a cancer cell that can be objectively measured and evaluated as an indicator of cancerous processes within the body. The term tumor marker was firstly coined in 1847 and presently there are more than 100 known different tumor markers [110]. Biomarkers have a great potential for screening and diagnostics because they are present in blood and provide information about the health condition [111]. In healthy individuals, the tumor marker concentration is comparatively

low level or even absent, while increased values can reveal development and/or progression of a disease [112]. Serum biomarkers providing key information about the disease are important for management of cancer patients since blood aspiration is only a moderately invasive procedure. There is clear need for early-stage cancer diagnostics, efficient treatment and posttreatment monitoring to avoid progress of the disease into advanced stages. Therefore there is an enormous demand for efficient less-invasive investigation *i.e.* analysis of cancer biomarkers in plasma/serum samples at low limit of detection [113].

> *Limit of Detection (LOD): the level of analyte that leads to a sensor signal which is statistically significantly different from the background signal obtained in the absence of the analyte. A frequently used definition of LOD is a concentration that gives a signal greater than three times the standard deviation of a blank sample consisting entirely of a matrix (S/N) = 3.*

The unique physico-chemical properties of MXenes make them a significant tool that can be employed in the cancer therapy (photothermal therapy, photodynamic therapy, radiation therapy, chemotherapy), cancer imaging (CT/MRI/PA imaging) as well as cancer theranostic applications [21].

5.2 MXene-based electrochemical nanobiosensors

Electrochemical biosensors are prospective tool of choice for an early-stage diagnostics of cancer diseases [114]. Electrochemical methods such as CV, CA, DPV, EIS, square wave voltammetry (SWV) provide a number of advantages. They are reliable, easy-to-use, affordable and highly sensitive and reliable [107, 115, 116]. Lab-on-chip biosensors are compact and portable miniaturized devices that can be employed in cancer biomarkers research leading to potential clinical applications. Biosensors employing surface nanoarchitectures with this type of detection offer attractive features including straightforward miniaturization, excellent LODs, robustness, small analyte volumes and the ability to be applied in turbid biofluids with optically absorbing and fluorescing compounds.

Single/few-layered MXene (Ti_3C_2) nanosheets were functionalized with (3-aminopropyl)triethoxysilane (APTES) to enable covalent attachment of bio-receptor onto *f*-Ti_3C_2-MXene for electrochemical detection of carcinoembryonic antigen (CEA) as a widely used tumor marker [77]. The ultrathin 2D nanosheets of single/multilayer MXene Ti_3C_2 with high density of functional groups brought in improved antibodies anchoring and faster access to analyte. The label-free aminosilane and bio-functionalized *f*-Ti_3C_2-MXene-based biosensor (BSA/anti-CEA/f-Ti_3C_2-MXene/GC) demonstrated LOD of 0.000018 ng mL^{-1} with sensitivity of 37.9 μA ng^{-1} mL cm^{-2} *per* decade (a linear detection range of 0.0001–2000 ng mL^{-1}) for CEA determination using hexaammineruthenium ($[Ru(NH_3)_6]^{3+}$) as a preferable redox probe and CV as a detection technique [77].

> *Carcinoembryonic antigen (CEA, molecular mass of 180–200 kDa) is a highly glycosylated cell surface protein consisting of approx. 60% carbohydrates, which attains elevated levels in a number malignancies, such as colorectal, breast and ovarian, gastric, liver and pancreatic cancer. Serum CEA is used in clinical research to identify early stages of disease, monitor tumor recurrence and metastatic disease. The normal range of serum CEA in healthy adults of non-smokers is below 2.5 ng mL^{-1} and in the serum of smokers below 5.0 ng mL^{-1}, but increases rapidly when normal cells become cancerous.*

Due to their excellent electrical conductivity and large specific surface area with a large number of potential attachment binding sites, 2D MXenes are also applied as

a conductive support for immobilization of aptamer probes. Wang *et al*. modified electrode surface with MXene for development of a MUC1 biosensor [117]. The ferrocene-labeled complementary DNA was bound onto MXene nanosheets to design a detection probe for electrochemical signal amplification. GCE was modified by electrodeposited AuNPs with MUC1 aptamer attached to the modified electrode *via* Au-S bonds. The modified electrode was blocked using bovine serum albumin (BSA) in order to resist non-specific interactions. Next, a detection probe was attached to the modified electrode *via* hybridization between complementary DNA and a MUC1 aptamer. Upon interaction of MUC1 with such an electrode, the detection probe was detached from the working electrode resulting in a decrease of an electrochemical signal (a signal-off response). This competitive aptasensor detected MUC1 with LOD of 0.33 pM with a linear range up to 10 mM. The relative standard deviation (RSD) of the peak current difference response was 1.43%, indicating that the aptasensor had good reproducibility. The peak current difference response of the aptasensor did not change much in ten days, indicating its acceptable stability [117].

Currently, there are more than 20 known types of mucins. They are encoded by MUC genes and represent high molecular weight glycoproteins expressed on epithelial cells. Aberrantly glycosylated mucins are expressed in cancer cells and serve as oncogenic molecules.

MicroRNAs (miRNAs) overexpression is a biomarker for a number of diseases including cardiovascular disorders, cancer, rheumatic diseases, diabetes, neurological disorders, liver diseases, kidney diseases, and immune dysfunction. The microRNAs (miRNAs) are biomolecules composed of 18–24 nucleotides and they play a key role in biological processes such as cell proliferation, apoptosis and tumorigenesis. Abnormal expression has been monitored in breast cancer as well as in other cancer types with observed blood stability. The miRNA-182 demonstrates tissue specificity and sequential expression in the different stages during lung cancer development or evolution. The miRNA-155 is overexpressed in human breast cancers.

The label-free strategy for the ultrasensitive detection of miRNA-182 was based on glassy carbon electrode (GCE) modified step-by-step by van der Waals forces and electrostatic interactions with MoS_2/Ti_3C_2, AuNPs, ssRNA [118]. BSA was used to block unbound gold particles surface and avoid nonspecific adsorption. The biosensor was able to determine miRNA-182 with LOD of 0.43 fM (a linear range of 1 fM - 0.1 nM) by DPV method [118]. The recovery was 105%, 95.3% and 93.0% for the concentration of 10^{-10} M, 10^{-12} M and 10^{-14} M of the analyte respectively, manifesting its effective detection of miRNA-182 in real sample [118].

Duan with co-workers [119] developed an impedimetric aptasensing strategy based on a novel zero dimensional (0D)/2D nanohybrid of $Ti_3C_2T_x$ nanosheets decorated with FePc QDs (denoted as $Ti_3C_2T_x$@using iron phthalocyanine quantum dots (FePcQDs)) for miRNA-155 detection. The miRNA-155 was established by applying impedimetric aptasensor with LOD of 4.3 aM (S/N = 3, a linear concentration range from 0.01 fM to 10 pM). The observed relative standard deviation (RSD) of the five aptasensors for detection of miRNA-155 was as low as 2.98%, demonstrating good reproducibility of the proposed aptasensor. Moreover, the signal remained 104% of the original signal after 15 days of storage, revealing a satisfactory stability of the present aptasensor [119].

Multiple (miRNA-21 and miRNA-141) and rapid (80 min) analysis of onco microRNAs in total plasma was carried out with combination of AuNPs (5 nm) decorated MXene as an electrode interface and a duplex-specific nuclease (DSN) as an amplification system applied onto home-made screen-printed gold electrode

(SPGE) [88]. As the initial step functionalization of two magnetic particles (MPs) with two different single-stranded DNAs (ssDNAs) was performed through labeling with methylene blue (MB) and ferrocene (Fc) that were partially complementary to the target miRNA. After the invasion of targets and amplification cycle, the released uncleaved DNA sequences harboring redox labels were hybridized with the electrochemical sensor platforms for subsequent measurements. To enhance the electrochemical signal, the SPGE was modified with the synthesized MXene-$Ti_3C_2T_x$ and patterned with AuNPs and further loaded with abundant ssDNAs (base) to provide a significantly higher electrochemical signal compared to the AuNP/Au electrodes (almost 4 orders of magnitude increase). The LODs of the biosensor exhibiting multiplex ability, antifouling activity and single mutation recognition for microRNA-21 and microRNA-141 detection reaching low LOD levels down to 204 aM and 138 aM (a wide linear range up to 50 nM), respectively. The synergic effect of combining MXene based electrochemical amplification and DSN target recycling, resulted in a short assay time of 80 min, a good assay reproducibility (RSD ≈ 4.7%) and stability of 95.2% and 97.1% of its initial signal values assigned to MB and Fc, respectively, after 4 weeks of storage [88].

Xu *et al*. [120] treated Ti_3C_2 MXene with NaOH and hydrogen peroxide in a Teflon lined stainless-steel autoclave by a simultaneous oxidation and alkalization resulting in the synthesized 3D sodium titanate nanoribbons (M-NTO) in order to overcome restacking of MXenes flakes. Such a composite offered fast electron transfer ability, high specific surface area and excellent biocompatibility by connection of 3D M-NTO with conductive poly(3,4-ethylenedioxythiophene) (PEDOT). AuNPs were electrodeposited in the next step on the surface of M-NTO-PEDOT for immobilization of antibodies against prostate specific antigen (PSA) for PSA detection. Assay reproducibility was high with RSD of 1.89% with satisfactory biosensor stability (84.2% of its original response after 2 weeks storage at 4°C). The label-free immunosensor could detect PSA with LOD of 0.03 pg. L^{-1} (S/N = 3) by DPV [120].

The prostate-specific antigen (PSA, 28.4 kDa) belongs to the tissue kallikrein-related family of peptidases and is also known as g-seminoprotein, kallikrein-3 or KLK3. PSA presenting a single-chain glycoprotein containing approximately 8% (by mass) of N-glycan with a single glycosylation site is produced by vesicles in prostate epithelial cells. Prostate cancer (PCa, adenocarcinoma or glandular cancer of the prostate gland) is the 2nd most abundant cancer type in men worldwide, with an estimated 1.1 million cases diagnosed in 2012 alone. The PSA level in health body is lower than 4 ng mL^{-1}.

In addition, PSA was sensitively detected with capacitance-based enzyme immunosensor [121] based on enzymatic biocatalytic precipitation of precipitate on interdigitated micro-comb electrode (IDE). AuNPs heavily functionalized with HRP and detection antibodies (HRP-Au-Ab_2) were utilized as the signal generating probe. Firstly, MXene dispersion in 1.0 wt % Nafion ethanol solution was dropped onto IDE to modify it. Next anti-PSA capture antibodies (Ab_1) were physically adsorbed onto the nanosheets. Subsequently PSA, HRP-Au-Ab_2 conjugates, H_2O_2 and HRP-tyramine conjugates were incubated step-by-step with the immunosensor at room temperature. The target PSA was determined with LOD of 0.031 ng mL^{-1} in a linear range up to 50 ng mL^{-1} with RSD of 10.7%, indicating good reproducibility [121].

Liu *et al*. [122] designed a "signal-on" photoelectrochemical (PEC) biosensor employing a $Ti_3C_2/BiVO_4$ Schottky junction for a signal generation for ultrasensitive detection of vascular endothelial growth $factor_{165}$ ($VEGF_{165}$) with LOD of 3.3 fM (a linear range of 10 fM - 100 nM). First, *in situ* synthesized

$Ti_3C_2/BiVO_4$ nanocomposite covered the surface of the electrode to produce an initial photocurrent signal. The T7 Exonuclease (T7 Exo)-assisted dual signal amplification strategy was applied to achieve improved sensitivity of the PEC sensor. With the target $VEGF_{165}$, the hairpin DNA (HP2), containing the aptamer of $VEGF_{165}$ can be specifically identified and opened to specifically recognize the exposed toehold of S1 on the magnetic bead, releasing the output DNA S2, S3, and S4. Further, T7 Exo was used to digest the recessed 5′ termini of double-stranded DNA (dsDNA). $VEGF_{165}$-HP2 complex was released for the next cycle, which can be converted to multiple output DNAs. Next, the output DNA hybridized with hairpin DNA (HP1) on the electrode to form a double-stranded structure, which provided a wonderful platform for the intercalation of methylene blue. Methylene blue effectively increased light absorption and promoted the electron transfer along the dsDNA, resulting in an enhanced PEC signal. The inter-assay and intra-assay RSD values were calculated to be 2.42% and 2.26%, respectively, illustrating the outstanding reproducibility of the biosensor [122].

The vascular endothelial growth factor (VEGF) is a biomarker with a molecular mass of 18–27 kDa and can be related to various cancer types for example brain, lung, gastrointestinal, hepatobiliary, renal, breast, ovarian. Normal level of VEGF in serum is ~ 220 pg mL^{-1}.

An impedimetric aptasensor based on the nanostructured multicomponent hybrid of $Ti_3C_2T_x$ nanosheets and phosphomolybdic acid (PMo_{12}) nanoparticles integrated by embedding within the polypyrrole (PPy) matrix ($PPy@Ti_3C_2T_x/PMo_{12}$) was utilized for detection of osteopontin (OPN) [53]. The $PPy@Ti_3C_2T_x/PMo_{12}$-based aptasensor estimated OPN with LOD of 0.98 fg mL^{-1} in a linear range of 0.05–10,000 pg. mL^{-1}. The biosensor exhibited low RSD of the assays of around 1.7% and during the biosensor offered also good operational stability [53].

Osteopontin (OPN, 41–75 kDa) known as a phosphoprotein regulates tumor metastasis and leads to cancer progression (breast, colon, liver, lung, ovarian, prostate). OPN plays an important role in tumor invasion, growth, angiogenesis, and metastasis by upregulating several signaling pathways. Normal level in serum is 16 ng mL^{-1}.

5.3 MXene-based optical nanobiosensors

Surface plasmon resonance (SPR) is a principal technique for *in situ* bioaffinity assays of various target (bio)molecules without a need for fluorescent or enzymatic labeling. SPR (bio)sensors could be developed with improved operational parameters by applying nanomaterials [123]. SPR detection platform offers beneficial advantages for the biosensing including label-free and real-time detection, high sensitivity and selectivity, ease of miniaturization and rapid detection making the technique well suited for bioassays.

Surface plasmon resonance (SPR) is optical sensing technology which can be used for health monitoring, early disease diagnosis, and environment safety. It has become a valuable tool for biological, chemical, and biomedical applications. It has been widely used in various biochemical and biosensing applications, particularly for enzyme detection, drug diagnostic, dsDNA hybridization, and applied as an immune sensor. SPR sensors are refractive index based sensors that can be experimentally implemented for real-time biosensing without the labeling of the analytes or bioreceptors.

It is an established high sensitivity platform for measuring minute concentrations of analyte and kinetics of biomolecular interactions. SPR generates an evanescent wave at the interface of two materials, when properly polarized incident light excites charge density oscillation (also called surface plasmons, SPs) supported by thin metal film deposited on the prism. However, SPR condition is established only after proper coupling of p-polarized incident wave with surface plasmon wave (SPW), when the frequency of evanescent wave matches the natural frequency of the SPW. SPR in reflection mode measures the resonance angle at a dip in reflectivity and a complete energy transfer from evanescent wave to SPW is achieved. Resonance angle is very sensitive to alteration of sensing medium refractive index (RI), i.e. on adsorption of analytes, which changes SPR condition. The sensitivity of the sensor is directly related to the resonance angle shift, which is sensitive to the modification of the RI of the sensing medium. In conventional SPR, a thin film of noble metal is used for SPs generation as well as adsorption of biomolecules or other analytes. Gold is a preferred interface, as it is non-oxidizing, corrosion-free, with substantial chemical stability, and shows stable adsorption of analytes with high sensitivity. However it shows a broad resonance curve causing reduction in detection accuracy. Silver (Ag) on the other hand shows higher accuracy through sharper reflectance curve but a poor chemical stability, as it is assumed to oxidize quickly on direct exposure to the atmosphere. Ag can be utilized efficiently in the SPR sensor if its oxidation can be avoided by using some protective layer over it. Conventional SPR sensor utilizing prism, metal layer and sensing medium offers smaller sensitivity.

Due to its absorption, a few-layer $Ti_3C_2T_x$ MXene can contribute to the improved sensitivity of SPR biosensors. Enhanced sensitivity by 16.8%, 28.4%, 46.3% and 33.6% was achieved for the proposed SPR biosensors based on Au with 4 layers, Ag with 7 layers, Al with 12 layers and Cu with 9 layers of $Ti_3C_2T_x$, respectively [124].

The platform based on prism/gold layer/MXene/WS_2/black phosphorus using monolayer of each nanomaterial was proved as a novel SPR sensing material with enhanced sensitivity of 15.6% compared to a bare metal film [125]. MXene-based composite, g-C_3N_4/MXene-AgNPs, including g-C_3N_4 as a photocatalyst, MXene as a co-catalyst and AgNPs as an electron mediator offered enhanced photocatalytic activity. The increased optical absorption and reduced band-gap energy due to the SPR effect of AgNPs deposited on such nanocomposite modified interface was observed [126].

Wu with co-workers [49] took advantage of hydrophilic and biocompatible Ti_3C_2 surface as a platform for making a nanohybrid consisting of multi-walled carbon nanotubes (MWCNTs)-polydopamine (PDA)-Ag nanoparticles (AgNPs) as a signal probe to develop SPR biosensor, that is easy to prepare, convenient to operate, and provides high sensitivity and selectivity. In order to obtain good orientation and immobilization of monoclonal anti-CEA antibody (Ab_1), synthesized Ti_3C_2/AuNPs composite was firstly decorated with staphylococcal protein A (SPA) to which Ab_1 was captured by affinity interaction through its Fc region. Polyclonal anti-CEA antibodies (Ab_2) were conjugated with a nanohybrid through Schiff-base reaction between amino residues and quinone groups of PDA. By introducing a MWPAg-Ab_2 conjugate to form a sandwich format, LOD of 0.07 fM was achieved for CEA detection (a dynamic range of 2×10^{-16} - 2×10^{-8} M). However, there are some limitations of such biosensing platform including time-consuming fabrication of the interfacial layer *prior* to analysis, but the biosensor exhibited good assay reproducibility with RSD below 5%. The stability of the fabricated sensing platform was also investigated by measuring the SPR responses to 10^{-12} M CEA concentration over the period of 7 days, during which the sensing platform was stored at 4°C. The developed biosensor lost 13% of its initial activity after storing for 7 days [49].

Wu *et al*. [127] utilized amino-functionalized N-Ti_3C_2-MXene-hollow gold nanoparticles (HGNPs)-staphylococcal protein A (SPA) complexes as a signal enhancer for CEA detection with LOD of 0.15 fM (a linear range of 0.001–1000 pM) at SPR (**Figure 3**). The SPR biosensor was stable (80% of the initial response

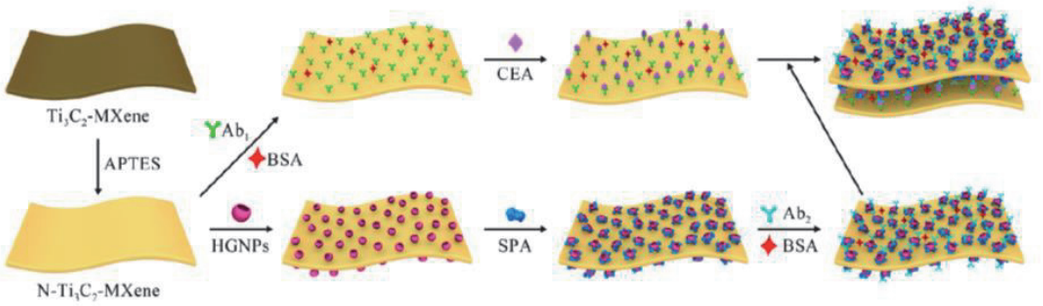

Figure 3.
Schematic of detection procedure of the prepared SPR biosensor. Reprinted with permission from ref. [127]. Copyright ACS, 2020.

after storage for 28 days), reproducible (average assay RSD less than 5%) and offering operational stability (84% of its initial activity after five reuse cycles) [127].

Among various investigation methods for detection of cancer biomarkers, fluorescence analysis methods, especially fluorescent nanoprobes based on "turn on" mechanism, are regarded as sensitive and reliable analytical tools for cancer diagnosis. The nanoprobes can be ideally stabilized in both extracellular and intracellular microenvironment and respond to multi-biomarkers with different spatial distributions to achieve multilayer information of diverse biomarkers range from cell membrane to the cytoplasm at a cellular level [128]. Wang with colleagues [128] investigated fluorescence quenching capacity of Ti_3C_2 MXenes for biosensing of dual biomarkers in single (MCF-7) living cells. A chimeric DNA-functionalized Ti_3C_2 probe was employed for real-time and multilayer simultaneous fluorescent imaging of plasma membrane glycoprotein MUC1 and cytoplasmic microRNA-21 at nM concentration *in vitro* (**Figure 4**). Ti_3C_2 MXene was decorated with polyacrylic acid to achieve high stabilization and dispersion of MXene with delivering functional groups were employed for covalent linkage of the bioreceptor (a dual signal-tagged chimeric DNA probe (dcDNA)) [128].

Guo *et al*. [129] fabricated Ti_3C_2 QDs (~4.2 nm in diameter) by a hydrothermal treatment with beneficial and excellent salt tolerance, anti-photobleaching and dispersion stability in aqueous solution. Ti_3C_2 QDs were applied as the fluorescent markers for fluorescent signal readout without and for sensitive fluorimetric analysis of alkaline phosphatase (ALP) activity with LOD of 0.02 U L^{-1}. Moreover, an accurate analysis of ALP by applying Ti_3C_2 QDs-based strategy for assays of AFP in the lysates of embryonic stem cells was also achieved by such a biosensor device [129].

> *Alkaline phosphatase (ALP), as an essential enzyme in phosphate metabolism, responsible for catalysis of the dephosphorylation of a variety of substrates. The abnormal level of serum ALP, as a crucial biomarker for clinical diagnostics, is closely related to various diseases, such as diabetes, hepatitis and prostatic cancer. In addition a high ALP activity is the traditional biomarker of pluripotent embryonic stem cells.*

A strand displacement dual amplification (SDDA) strategy was developed by Chen *et al*. [130] for simultaneous detection of multiple miRNAs analytes in a cell lysate using a unique single strand-double strand-single strand DNA (sdsDNA) probe, which was generated by the target recognition probe hybridizing with the site region probe. The fluorescence resonance energy transfer (FRET) assay was used for highly photostable, specific and sensitive detection of miRNAs with LOD

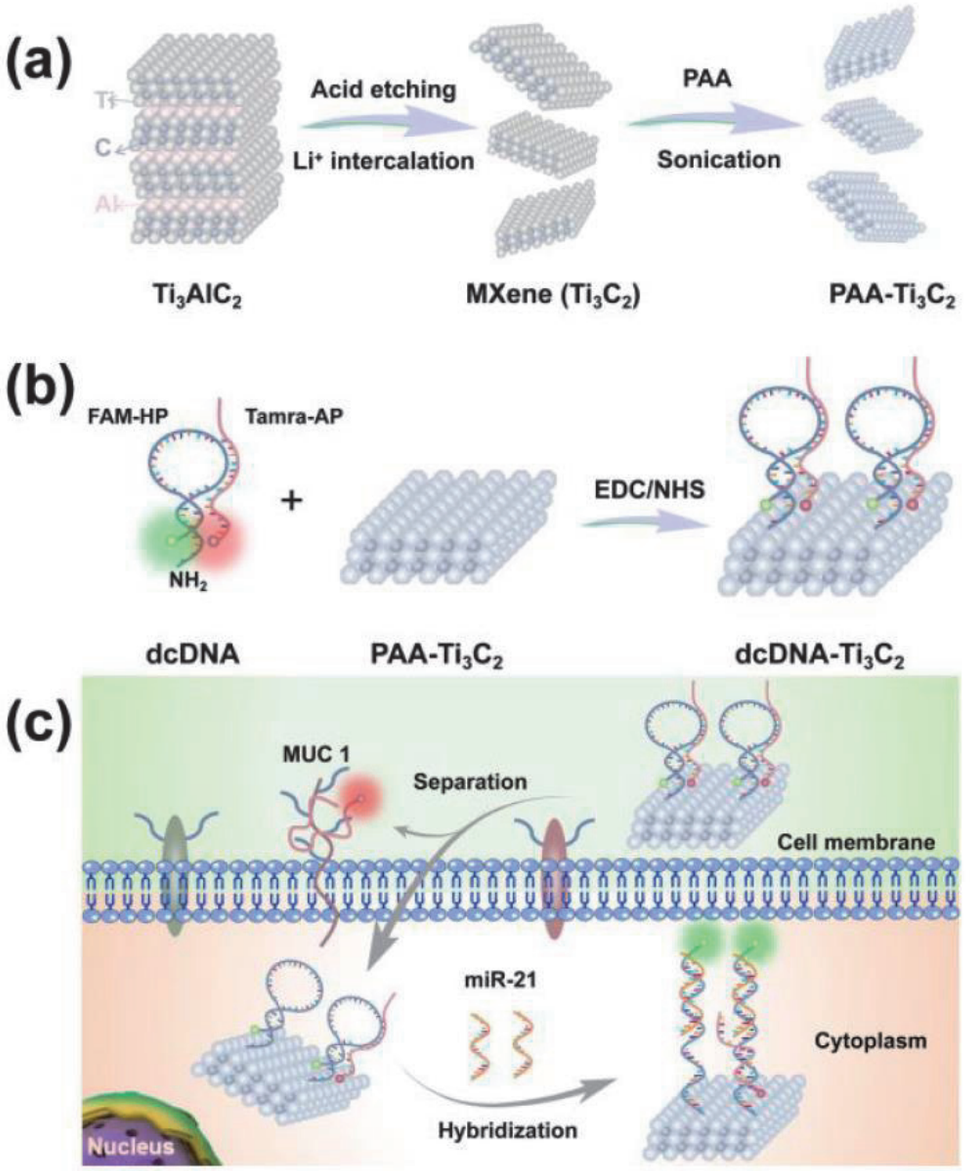

Figure 4.
(a) Illustration of the fabrication of the Ti_3C_2 MXenes and PAA-Ti_3C_2. (b) the construction of the dcDNA-Ti_3C_2 composite nanoprobe. (c) Multilayer imaging of plasma membrane glycoproteins MUC1 and cytoplasmic miR-21 using the dcDNA-Ti_3C_2 composite nanoprobe. Reprinted with permission from ref. [128]. Copyright ACS, 2019.

of 0.5 fM and 0.85 fM for miRNA-21 and miRNA-10b, respectively (a linear range from 5 fM to 100 pM) [130].

PSA was the both qualitatively and quantitatively examined through a sandwich-type immunoreaction and a photothermal measurement by applying Ti_3C_2 MXene quantum dots (QDs)-encapsulated liposome with a high photothermal efficiency [131]. Ti_3C_2 MXene QDs as the innovative photothermal signal beacons were entrapped in the liposome for the labeling of the secondary antibody on the surface. The sandwich-type assay was carried out by coupling a low-cost microplate with a homemade 3D printed device. Under NIR-laser irradiation of 808 nm, Ti_3C_2 MXene QDs converted the light energy into heat, and the shift in the temperature correlating with the analyte concentration. LOD of 0.4 ng mL^{-1} for PSA was obtained by a near-infrared (NIR) photothermal immunoassay (a linear range of 1.0 ng mL^{-1} - 50 ng mL^{-1}). The portable equipment employing a portable NIR imaging camera was able to

collect the visual thermal data for semi-quantitative analysis of target PSA within 3 min [131].

Liposome, a target-responsive nanomaterial containing a bilayer of phospholipids with the spherical structure, is promising due to its superior biocompatibility, versatility of surface modification, operability of dimensional control and large-volume internal loading. The functional liposome acts as the biological signal amplifier by encapsulating numerous signal molecules and binding with biological recognition molecules like DNA, enzyme, protein and nanomaterial.

5.4 Detection of exosomes as a source of cancer biomarkers by applying 2D MXenes

Exosomes as type of endosome-derived cell-secreted vesicles with the structure of a lipid bilayer membrane are responsible for signal transduction in intercellular communication and extracellular matrix remodeling. In addition exosomes can also carry cargo affecting neighboring cells and they can form pre-metastatic niches [115]. Thus, exosomes are behind localized tumor development, progression and induction of distant tumors forming metastasis. The fact, that a substantially higher cellular activity of tumor cells results in the production of a greater number of exosomes than in normal/healthy cells, makes them hot candidates for cancer diagnostics in itself [115].

Exosomes are naturally produced biological nanoparticles, with their size usually defined in the range from ~ 30 nm up to 100 nm or sometimes up to 200 nm. Other types of extracellular vesicles (EVs) include microvesicles (50–1000 nm, which bud directly off the plasma membrane), ectosomes (vesicles assembled at and released from a plasma membrane), shedding vesicles, microparticles and apoptotic vesicles (500–2000 nm, which bud off the membrane of cells undergoing apoptosis).

Electrochemiluminescence (ECL) as an upcoming technique joining the benefits of both electrochemistry and chemiluminescence, has been widely applied for biomarker analysis thanks to its high sensitivity, short response time and low background signal [132]. A biosensor based on the application of MXene and ECL was developed for sensitive detection of exosomes [133]. First, MXene ($\zeta \sim -50$ mV) was modified by polyethyleneimine (PEI) ($\zeta \sim +55$ mV) through electrostatic interactions to prepare an MXene/PEI nanocomposite ($\zeta \sim 80$ mV). This positively charged nanocomposite was subsequently used in covalent immobilization of an aptamer against CD63 protein, which is present on the surface of the exosomes using an amine-coupling chemistry. In an effort to detect exosomes, the GCE was modified by AuNPs, which were next modified by ethylenediamine. In addition, free -NH_2 groups of ethylenediamine were activated by EDC/NHS to deposit a polymer, which was finally used for covalent immobilization of an aptamer against the EpCAM protein present on the surface of the exosomes. The signal was generated upon completion of the sandwich configuration as shown in **Figure 5**. The biosensor was most sensitive towards exosomes produced by a breast cancer cell line MCF-7, followed by a human liver cancer cell line HepG2 and a melanoma cell line B16. Exosomes released from the MCF-7 cell line were detected in the concentration range from 500 to 5×10^6 particles μL^{-1} with LOD of 125 particles μL^{-1}, which was more than 100 times lower than the conventional ELISA method. The biosensor exhibited an excellent performance by analysis of spiked serum samples with recovery indices of 95–104% [133]. In the later research of the same group, it was shown that, besides CD63 and EpCAM, other proteins

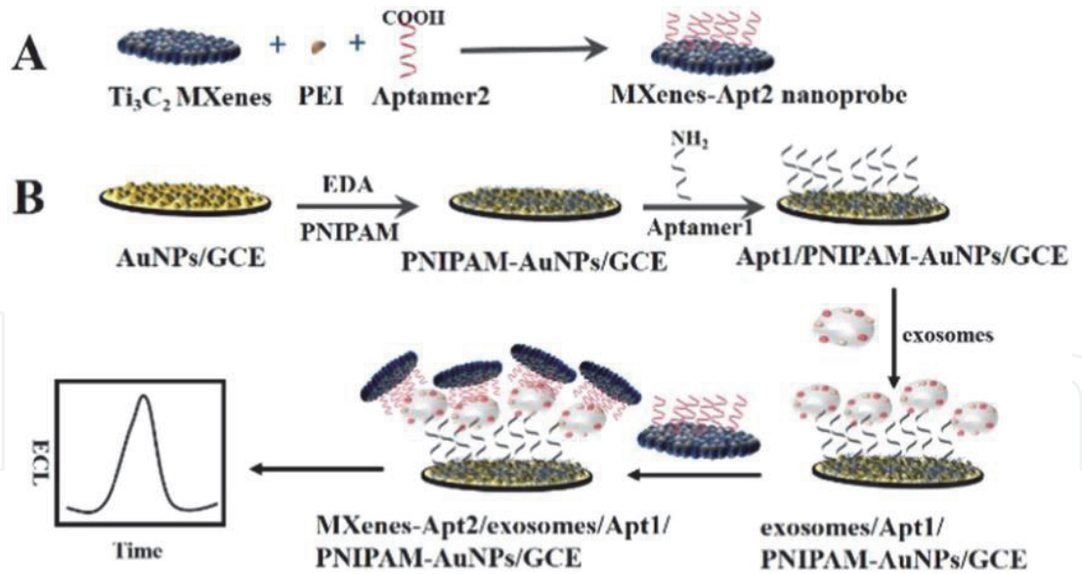

Figure 5.
The principle of the ECL biosensor for exosomes activity detection signal amplification strategy. Reprinted with permission from Ref. [134]. Copyright ACS, 2018.

present on the surface of the exosome can be targeted by DNA aptamers, including PSMA and PTK-7 [134]. Such a biosensor offered highly reproducible assays with RSD of 1.2% and 3.9% for detection of 10^8 and 10^9 exosomes mL^{-1}, respectively [134].

Another MXene-based biosensor for the detection of exosomes was prepared by Fang *et al*. [135] GCE was modified by SiNPs and ionic liquid with a final modification of the interface by EpCAM aptamers. In order to detect exosomes, a sandwich configuration was formed by a final incubation with a nanohybrid consisting of MXene modified by black phosphorus quantum dots, $Ru(bpy)_3^{2+}$ and anti-CD63 antibodies. In addition to the ECL detection of exosomes, such a configuration also made photothermal assays possible. The ECL biosensor could detect exosomes down to 37 particles μL^{-1} with a linear range of up to 5×10^7 particles μL^{-1}. The stability of the constructed biosensor was investigated by measuring 1.1×10^2 exosomes μL^{-1}. The ECL intensity kept a relatively stable value under sequential 10 cyclic scans with relative standard deviation (RSD) of 1.1% [135].

6. Conclusions

The novel 2D nanomaterial MXene has a potential to significantly influence the field of biosensing including affinity-based biosensors with expected exponential increase in related works to be published in the years to come. MXene-based biosensors offer adequate sensitivity required for detection of cancer biomarkers present in blood down to ng mL^{-1} level or better (**Table 1**). However a great deal of effort needs to be invested into finding proper decorating strategies for MXene to simultaneously allow immobilization of biomolecules, but at the same time providing resistance towards non-specific protein binding. Matching this criteria, affinity MXene-based biosensors can be applied for analysis of complex samples such as blood serum or plasma [23]. Point-of-care tests (POC) employing MXene/based devices represent promising candidates with benefits such as adaptability in different/adverse environment,

Target biomarker	Biosensor architecture	Detection method	LOD	Linear range	Reference
CEA	BSA/anti-CEA/f-Ti_3C_2-MXene/GC	Electrochemical/ CV	0.000018 ng mL^{-1}	0.0001–2000 ng mL^{-1}	[77]
CEA	Ti_3C_2MXene/AuNPs/SPA/Ab_1 and MWCNTs-PDA-AgNPs/Ab_2	SPR	0.07 fM	2×10^{-16} - 2×10^{-8} M	[49]
CEA	Ab_2-conjugated SPA/HGNPs/N-Ti_3C_2-MXene	SPR	0.15 fM	0.001–1000 pM	[127]
MUC1	cDNA-Fc/MXene/Apt/Au/ GCE	Electrochemical/ DPV	0.33 pM	1.0 pM - 10 mM	[117]
miRNA-182	BSA/ssRNA/ AuNPs/ MoS_2/Ti_3C_2/GCE	Electrochemical/ DPV	0.43 fM	1 fM - 0.1 nM	[118]
miRNA-155	cDNA/$Ti_3C_2T_x$@ FePcQDs/AE	Electrochemical/ EIS	4.3 aM	0.01 fM - 10 pM	[119]
miRNA-21 and miRNA-141	ssDNAs/AuNP@ MXene/SPGE	Electrochemical/ DPV	204 aM (miRNA-21) and 138 aM (miRNA-141)	500 aM - 50 nM	[88]
PSA	BSA/anti-PSA/AuNPs-M-NTO-PEDOT/GCE	Electrochemical/ DPV	0.03 pg. L^{-1}	0.0001–20 ng mL^{-1}	[120]
PSA	HRP-Au-Ab_2-PSA-Ab_1-MXene/IDE	Electrochemical/ EIS, CV	0.031 ng mL^{-1}	0.1–50 ng mL^{-1}	[121]
$VEGF_{165}$	MB/DNA/HT/HP1/AuNPs/Ti_3C_2/$BiVO_4$/GCE	Photoelectro-chemical	3.3 fM	10 fM - 100 nM	[122]
OPN	Apt/PPy@$Ti_3C_2T_x$/ PMo_{12}/AE	Electrochemical/ EIS	0.98 fg mL^{-1}	0.05–10,000 pg. mL^{-1}	[53]
Exosomes	ECL probe - (MXenesBPQDs@Ru(dcbpy)$_3^{2+}$-PEI-Ab_{CD63} exosomes/Apt/ILs/SiO_2 NUs/GCE	ECL	37.0 particles μL^{-1}	1.1×10^2–1.1×10^7 particles μL^{-1}	[135]
Exosomes	MXenes-Apt2/exosomes/Apt1/PNIPAMAuNPs/ GCE	ECL	125 particles μL^{-1}	5×10^2–5×10^6 particles μL^{-1}	[97]
Exosomes	Cy3 labeled CD63 aptamer (Cy3-CD63 aptamer)/ Ti_3C_2 MXenes	Ratiometric fluorescence resonance	1.4×10^3 particles mL^{-1}	10^4–10^9 particles mL^{-1}	[134]
miRNA-21 and miRNA-10b	DNA-$NaYF_4$:Yb,Tm/Er UCNPs and Ti_3C_2 nanosheets	Fluorescence - fluorescence resonance energy transfer (FRET) assay	0.62 fM (miRNA-21) and 0.85 fM (miRNA-10b)	5 fM - 100 pM	[130]

Table 1.
Key characteristics of MXene-based nanobiosensors for detection of cancer biomarkers.

automation of tests, reduced cost, miniaturization, interference-free detection, *etc*. [50, 81, 136, 137].

Acknowledgements

The authors would like to acknowledge financial support from the Slovak Research and Development Agency APVV 17–0300 and from projects granted by the Ministry of Health of the Slovak Republic No. 2018/23-SAV-1 and 2019/68-CHÚSAV-1. This book chapter was supported by Qatar University Grant IRCC-2020-004. The statements made herein are solely the responsibility of the authors.

Abbreviations

Ab_1	monoclonal anti-CEA antibody, monoclonal mouse anti-human PSA capture antibody
Ab_2	polyclonal anti-CEA antibody, polyclonal rabbit anti-human PSA detection antibody
AE	bare Au electrode
AgNPs	Ag nanoparticles
anti-CEA	carcinoembryonic antibody monoclonal antibody
Apt	MUC1 aptamer;
Au, AuNPs	Au nanoparticles
BPQDs	black phosphorous quantum dots
BSA	bovine serum albumin
CEA	carcinoembryonic antigen
CV	cyclic voltammetry
cDNA	complementary deoxyribonucleic acid
cDNA-Fc	ferrocene-labeled complementary deoxyribonucleic acid
DPV	differential pulse voltammetry
EIS	electrochemical impedance spectroscopy
f-Ti_3C_2-MXene	MXene functionalized with aminosilane
FePcQDs	phthalocyanine quantum dots
GC, GCE	glassy carbon electrode
HGNPs	hollow gold nanoparticles
HP1	hairpin DNA
HRP	horseradish peroxidase
HT	hexanethiol
IDE	interdigitated microcomb electrode
IL	ionic liquid (1-carboxymehyl-3-methylimidazolium chloride)
MB	methylene blue
miRNA	microRNA
M-NTO	3D sodium titanate nanoribbons
MUC1	mucin1
MWCNTs	multi-walled carbon nanotubes
N − Ti_3C_2-MXene	amino-functionalized Ti_3C_2-MXene
PDA	polydopamine
PEDOT	poly(3,4-ethylenedioxythiophene)
PMo_{12}	phosphomolybdic acid
PNIPAM	Poly (N-isopropylacrylamide), carboxylic acid
PPy	polypyrrole
ssDNAs	single-stranded DNAs

PSA	prostate specific antigen
SiO_2 NUs	SiO_2 nanourchin
SPA	staphylococcal protein A
SPGE	screen-printed gold electrode
SPR	surface plasmon resonance
UCNPs	upconversion nanophosphors
$VEGF_{165}$	vascular endothelial growth factor 165

Author details

Lenka Lorencova[1], Kishor Kumar Sadasivuni[2], Peter Kasak[2] and Jan Tkac[1]*

1 Institute of Chemistry, Slovak Academy of Sciences, Bratislava, Slovak Republic

2 Center for Advanced Materials, Qatar University, Doha, Qatar

*Address all correspondence to: jan.tkac@savba.sk

References

[1] Novoselov, K. S.; Jiang, D.; Schedin, F.; Booth, T. J.; Khotkevich, V. V.; Morozov, S. V.; Geim, A. K. Two-dimensional atomic crystals. *Proc. Natl. Acad. Sci. U.S.A.* **2005,** *102*, 10451.

[2] Geim, A. K.; Novoselov, K. S. The rise of graphene. *Nat. Mater.* **2007,** *6*, 183–191.

[3] Duncan, C.; Roddie, H. Dendritic cell vaccines in acute leukaemia. *Best Pract. Res. Clin. Heaematol.* **2008,** *21*, 521–541.

[4] Sun, Y.; Gao, S.; Lei, F.; Xiao, C.; Xie, Y. Ultrathin Two-Dimensional Inorganic Materials: New Opportunities for Solid State Nanochemistry. *Acc. Chem. Res.* **2015,** *48*, 3–12.

[5] Chen, Y.; Tan, C.; Zhang, H.; Wang, L. Two-dimensional graphene analogues for biomedical applications. *Chem. Soc. Rev.* **2015,** *44*, 2681–2701.

[6] GÜRbÜZ, B.; Ayan, S.; Bozlar, M.; ÜStÜNdaĞ, C. B. Carbonaceous nanomaterials for phototherapy: a review. *Emergent Materials* **2020,** *3*, 479–502.

[7] Abdo, G. G.; Zagho, M. M.; Khalil, A. Recent advances in stimuli-responsive drug release and targeting concepts using mesoporous silica nanoparticles. *Emergent Materials* **2020,** *3*, 407–425.

[8] Khan, K.; Tareen, A. K.; Aslam, M.; Wang, R.; Zhang, Y.; Mahmood, A.; Ouyang, Z.; Zhang, H.; Guo, Z. Recent developments in emerging two-dimensional materials and their applications. *J. Mater. Chem. C* **2020,** *8*, 387–440.

[9] Ghidiu, M.; Lukatskaya, M. R.; Zhao, M.-Q.; Gogotsi, Y.; Barsoum, M. W. Conductive two-dimensional titanium carbide 'clay' with high volumetric capacitance. *Nature* **2014,** *516*, 78–81.

[10] Naguib, M.; Mashtalir, O.; Carle, J.; Presser, V.; Lu, J.; Hultman, L.; Gogotsi, Y.; Barsoum, M. W. Two-Dimensional Transition Metal Carbides. *ACS Nano* **2012,** *6*, 1322–1331.

[11] Naguib, M.; Gogotsi, Y. Synthesis of Two-Dimensional Materials by Selective Extraction. *Acc. Chem. Res.* **2015,** *48*, 128–135.

[12] Mashtalir, O.; Naguib, M.; Mochalin, V. N.; Dall'Agnese, Y.; Heon, M.; Barsoum, M. W.; Gogotsi, Y. Intercalation and delamination of layered carbides and carbonitrides. *Nat. Commun.* **2013,** *4*, 1716.

[13] Naguib, M.; Kurtoglu, M.; Presser, V.; Lu, J.; Niu, J.; Heon, M.; Hultman, L.; Gogotsi, Y.; Barsoum, M. W. Two-Dimensional Nanocrystals Produced by Exfoliation of Ti3AlC2. *Adv. Mater.* **2011,** *23*, 4248–4253.

[14] Pang, J.; Mendes, R. G.; Bachmatiuk, A.; Zhao, L.; Ta, H. Q.; Gemming, T.; Liu, H.; Liu, Z.; Rummeli, M. H. Applications of 2D MXenes in energy conversion and storage systems. *Chem. Soc. Rev.* **2019,** *48*, 72–133.

[15] Bu, F.; Zagho, M. M.; Ibrahim, Y. S.; Ma, B.; Elzatahry, A. A.; Zhao, D. Porous MXenes: Synthesis, structures, and applications. *Nano Today* **2020,** *30*, 100803.

[16] Wang, X.; Salari, M.; Jiang, D.-e.; Chapman Varela, J.; Anasori, B.; Wesolowski, D. J.; Dai, S.; Grinstaff, M. W.; Gogotsi, Y. Electrode material–ionic liquid coupling for electrochemical energy storage. *Nature Reviews Materials* **2020**.

[17] Shahzad, F.; Alhabeb, M.; Hatter, C. B.; Anasori, B.; Man Hong, S.; Koo, C. M.; Gogotsi, Y. Electromagnetic interference shielding with 2D

transition metal carbides (MXenes). *Science* **2016,** *353*, 1137.

[18] Iqbal, A.; Shahzad, F.; Hantanasirisakul, K.; Kim, M.-K.; Kwon, J.; Hong, J.; Kim, H.; Kim, D.; Gogotsi, Y.; Koo, C. M. Anomalous absorption of electromagnetic waves by 2D transition metal carbonitride Ti3CNTx (MXene). *Science* **2020,** *369*, 446.

[19] Rasool, K.; Pandey, R. P.; Rasheed, P. A.; Buczek, S.; Gogotsi, Y.; Mahmoud, K. A. Water treatment and environmental remediation applications of two-dimensional metal carbides (MXenes). *Mater. Today* **2019,** *30*, 80–102.

[20] Ibrahim, Y.; Kassab, A.; Eid, K.; M Abdullah, A.; Ozoemena, K. I.; Elzatahry, A. Unveiling Fabrication and Environmental Remediation of MXene-Based Nanoarchitectures in Toxic Metals Removal from Wastewater: Strategy and Mechanism. *Nanomaterials (Basel)* **2020,** *10*, 885.

[21] Sundaram, A.; Ponraj, J. S.; Wang, C.; Peng, W. K.; Manavalan, R. K.; Dhanabalan, S. C.; Zhang, H.; Gaspar, J. Engineering of 2D transition metal carbides and nitrides MXenes for cancer therapeutics and diagnostics. *J. Mater. Chem. B* **2020,** *8*, 4990–5013.

[22] Kalambate, P. K.; Gadhari, N. S.; Li, X.; Rao, Z.; Navale, S. T.; Shen, Y.; Patil, V. R.; Huang, Y. Recent advances in MXene–based electrochemical sensors and biosensors. *Trends Anal. Chem.* **2019,** *120*, 115643.

[23] Lorencova, L.; Gajdosova, V.; Hroncekova, S.; Bertok, T.; Blahutova, J.; Vikartovska, A.; Parrakova, L.; Gemeiner, P.; Kasak, P.; Tkac, J. 2D MXenes as Perspective Immobilization Platforms for Design of Electrochemical Nanobiosensors. *Electroanal.* **2019,** *31*, 1833–1844.

[24] Naguib, M.; Mochalin, V. N.; Barsoum, M. W.; Gogotsi, Y. Two-Dimensional Materials: 25th Anniversary Article: MXenes: A New Family of Two-Dimensional Materials. *Adv. Mater.* **2014,** *26*, 982–982.

[25] Michael, J.; Qifeng, Z.; Danling, W. Titanium carbide MXene: Synthesis, electrical and optical properties and their applications in sensors and energy storage devices. *Nanomater. Nanotechnol.* **2019,** *9*, 1847980418824470.

[26] Gund, G. S.; Park, J. H.; Harpalsinh, R.; Kota, M.; Shin, J. H.; Kim, T.-i.; Gogotsi, Y.; Park, H. S. MXene/Polymer Hybrid Materials for Flexible AC-Filtering Electrochemical Capacitors. *Joule* **2019,** *3*, 164–176.

[27] Er, D.; Li, J.; Naguib, M.; Gogotsi, Y.; Shenoy, V. B. Ti3C2 MXene as a High Capacity Electrode Material for Metal (Li, Na, K, Ca) Ion Batteries. *ACS Appl. Mater. Interf.* **2014,** *6*, 11173–11179.

[28] Come, J.; Black, J. M.; Lukatskaya, M. R.; Naguib, M.; Beidaghi, M.; Rondinone, A. J.; Kalinin, S. V.; Wesolowski, D. J.; Gogotsi, Y.; Balke, N. Controlling the actuation properties of MXene paper electrodes upon cation intercalation. *Nano Energy* **2015,** *17*, 27–35.

[29] Lukatskaya, M. R.; Mashtalir, O.; Ren, C. E.; Dall'Agnese, Y.; Rozier, P.; Taberna, P. L.; Naguib, M.; Simon, P.; Barsoum, M. W.; Gogotsi, Y. Cation Intercalation and High Volumetric Capacitance of Two-Dimensional Titanium Carbide. *Science* **2013,** *341*, 1502.

[30] Li, Q.; Zhou, J.; Li, F.; Sun, Z. Novel MXene-based hierarchically porous composite as superior electrodes for Li-ion storage. *Applied Surface Science* **2020,** *530*.

[31] Jia, X.; Shen, B.; Zhang, L.; Zheng, W. Construction of shape-memory

carbon foam composites for adjustable EMI shielding under self-fixable mechanical deformation. *Chemical Engineering Journal* **2021,** *405*.

[32] Rajavel, K.; Hu, Y.; Zhu, P.; Sun, R.; Wong, C. MXene/metal oxides-Ag ternary nanostructures for electromagnetic interference shielding. *Chemical Engineering Journal* **2020,** *399*.

[33] Li, Y.; Lu, Z.; Xin, B.; Liu, Y.; Cui, Y.; Hu, Y. All-solid-state flexible supercapacitor of Carbonized MXene/ Cotton fabric for wearable energy storage. *Applied Surface Science* **2020,** *528*.

[34] Miao, J.; Zhu, Q.; Li, K.; Zhang, P.; Zhao, Q.; Xu, B. Self-propagating fabrication of 3D porous MXene-rGO film electrode for high-performance supercapacitors. *Journal of Energy Chemistry* **2021,** *52*, 243–250.

[35] Luo, Y.; Tian, Y.; Tang, Y.; Yin, X.; Que, W. 2D hierarchical nickel cobalt sulfides coupled with ultrathin titanium carbide (MXene) nanosheets for hybrid supercapacitors. *Journal of Power Sources* **2021,** *482*.

[36] Yang, Z.; Jiang, L.; Wang, J.; Liu, F.; He, J.; Liu, A.; Lv, S.; You, R.; Yan, X.; Sun, P.; Wang, C.; Duan, Y.; Lu, G. Flexible resistive NO2 gas sensor of three-dimensional crumpled MXene Ti3C2Tx/ZnO spheres for room temperature application. *Sensors and Actuators B: Chemical* **2021,** *326*, 128828.

[37] Deshmukh, K.; Kovářík, T.; Khadheer Pasha, S. K. State of the art recent progress in two dimensional MXenes based gas sensors and biosensors: A comprehensive review. *Coordination Chemistry Reviews* **2020,** *424*, 213514.

[38] Wang, D.; Wang, L.; Lou, Z.; Zheng, Y.; Wang, K.; Zhao, L.; Han, W.; Jiang, K.; Shen, G. Biomimetic, biocompatible and robust silk Fibroin-MXene film with stable 3D cross-link structure for flexible pressure sensors. *Nano Energy* **2020,** *78*.

[39] Wang, L.; Zhang, M.; Yang, B.; Tan, J.; Ding, X. Highly Compressible, Thermally Stable, Light-Weight, and Robust Aramid Nanofibers/Ti3AlC2 MXene Composite Aerogel for Sensitive Pressure Sensor. *ACS nano* **2020,** *14*, 10633–10647.

[40] Wang, X.; Li, M.; Yang, S.; Shan, J. A novel electrochemical sensor based on TiO2–Ti3C2TX/CTAB/chitosan composite for the detection of nitrite. *Electrochimica Acta* **2020,** *359*.

[41] Abdul Rasheed, P.; Pandey, R. P.; Gomez, T.; Jabbar, K. A.; Prenger, K.; Naguib, M.; Aïssa, B.; Mahmoud, K. A. Nb-based MXenes for efficient electrochemical sensing of small biomolecules in the anodic potential. *Electrochemistry Communications* **2020,** *119*, 106811.

[42] Tu, X.; Gao, F.; Ma, X.; Zou, J.; Yu, Y.; Li, M.; Qu, F.; Huang, X.; Lu, L. Mxene/carbon nanohorn/β-cyclodextrin-Metal-organic frameworks as high-performance electrochemical sensing platform for sensitive detection of carbendazim pesticide. *Journal of Hazardous Materials* **2020,** *396*.

[43] Kalambate, P. K.; Dhanjai; Sinha, A.; Li, Y.; Shen, Y.; Huang, Y. An electrochemical sensor for ifosfamide, acetaminophen, domperidone, and sumatriptan based on self-assembled MXene/MWCNT/chitosan nanocomposite thin film. *Microchimica Acta* **2020,** *187*.

[44] Huang, H.; Jiang, R.; Feng, Y.; Ouyang, H.; Zhou, N.; Zhang, X.; Wei, Y. Recent development and prospects of surface modification and biomedical applications of MXenes. *Nanoscale* **2020,** *12*, 1325–1338.

[45] Rafieerad, A.; Yan, W.; Amiri, A.; Dhingra, S. Bioactive and trackable

MXene quantum dots for subcellular nanomedicine applications. *Materials and Design* **2020,** *196*.

[46] Nie, Y.; Huang, J.; Ma, S.; Li, Z.; Shi, Y.; Yang, X.; Fang, X.; Zeng, J.; Bi, P.; Qi, J.; Wang, S.; Xia, Y.; Jiao, T.; Li, D.; Cao, M. MXene-hybridized silane films for metal anticorrosion and antibacterial applications. *Applied Surface Science* **2020,** *527*.

[47] Wang, W.; Feng, H.; Liu, J.; Zhang, M.; Liu, S.; Feng, C.; Chen, S. A photo catalyst of cuprous oxide anchored MXene nanosheet for dramatic enhancement of synergistic antibacterial ability. *Chemical Engineering Journal* **2020,** *386*.

[48] Zheng, K.; Li, S.; Jing, L.; Chen, P. Y.; Xie, J. Synergistic Antimicrobial Titanium Carbide (MXene) Conjugated with Gold Nanoclusters. *Advanced Healthcare Materials* **2020**.

[49] Wu, Q.; Li, N.; Wang, Y.; liu, Y.; Xu, Y.; Wei, S.; Wu, J.; Jia, G.; Fang, X.; Chen, F.; Cui, X. A 2D transition metal carbide MXene-based SPR biosensor for ultrasensitive carcinoembryonic antigen detection. *Biosens. Bioelectron.* **2019,** *144*.

[50] Liu, J.; Jiang, X.; Zhang, R.; Zhang, Y.; Wu, L.; Lu, W.; Li, J.; Li, Y.; Zhang, H. MXene-Enabled Electrochemical Microfluidic Biosensor: Applications toward Multicomponent Continuous Monitoring in Whole Blood. *Adv. Funct. Mater.* **2019,** *29*, 1807326.

[51] Shang, L.; Wang, X.; Zhang, W.; Jia, L. P.; Ma, R. N.; Jia, W. L.; Wang, H. S. A dual-potential electrochemiluminescence sensor for ratiometric detection of carcinoembryonic antigen based on single luminophor. *Sensors and Actuators, B: Chemical* **2020,** *325*.

[52] Medetalibeyoglu, H.; Kotan, G.; Atar, N.; Yola, M. L. A novel and ultrasensitive sandwich-type electrochemical immunosensor based on delaminated MXene@AuNPs as signal amplification for prostate specific antigen (PSA) detection and immunosensor validation. *Talanta* **2020,** *220*, 121403.

[53] Zhou, S.; Gu, C.; Li, Z.; Yang, L.; He, L.; Wang, M.; Huang, X.; Zhou, N.; Zhang, Z. Ti3C2Tx MXene and polyoxometalate nanohybrid embedded with polypyrrole: Ultra-sensitive platform for the detection of osteopontin. *Appl. Surf. Sci.* **2019,** *498*.

[54] Soomro, R. A.; Jawaid, S.; Kalawar, N. H.; Tunesi, M.; Karakuş, S.; Kilislioğlu, A.; Willander, M. In-situ engineered MXene-TiO2/BiVO4 hybrid as an efficient photoelectrochemical platform for sensitive detection of soluble CD44 proteins. *Biosensors and Bioelectronics* **2020,** *166*, 112439.

[55] Yang, X.; Feng, M.; Xia, J.; Zhang, F.; Wang, Z. An electrochemical biosensor based on AuNPs/Ti3C2 MXene three-dimensional nanocomposite for microRNA-155 detection by exonuclease III-aided cascade target recycling. *Journal of Electroanalytical Chemistry* **2020,** *878*.

[56] Barsoum, M.; Radovic, M. Mechanical Properties of the MAX Phases. *Annu. Rev. Mater. Res.* **2011,** *41*, 195–227.

[57] Halim, J.; Lukatskaya, M. R.; Cook, K. M.; Lu, J.; Smith, C. R.; Näslund, L.-Å.; May, S. J.; Hultman, L.; Gogotsi, Y.; Eklund, P.; Barsoum, M. W. Transparent Conductive Two-Dimensional Titanium Carbide Epitaxial Thin Films. *Chem. Mater.* **2014,** *26*, 2374–2381.

[58] Tang, H.; Hu, Q.; Zheng, M.; Chi, Y.; Qin, X.; Pang, H.; Xu, Q. MXene–2D layered electrode materials for energy storage. *Prog. Nat. Sci: Mater. International.* **2018,** *28*, 133–147.

[59] Hope, M. A.; Forse, A. C.; Griffith, K. J.; Lukatskaya, M. R.; Ghidiu, M.; Gogotsi, Y.; Grey, C. P. NMR reveals the surface functionalisation of Ti3C2 MXene. *Phys. Chem. Chem. Phys.* **2016,** *18*, 5099–5102.

[60] Gajdosova, V.; Lorencova, L.; Prochazka, M.; Omastova, M.; Micusik, M.; Prochazkova, S.; Kveton, F.; Jerigova, M.; Velic, D.; Kasak, P.; Tkac, J. Remarkable differences in the voltammetric response towards hydrogen peroxide, oxygen and Ru (NH3)63+ of electrode interfaces modified with HF or LiF-HCl etched Ti3C2Tx MXene. *Microchim. Acta* **2019,** *187*, 52.

[61] Lipatov, A.; Alhabeb, M.; Lukatskaya, M. R.; Boson, A.; Gogotsi, Y.; Sinitskii, A. Effect of Synthesis on Quality, Electronic Properties and Environmental Stability of Individual Monolayer Ti3C2 MXene Flakes. *Adv. Electron. Mater.* **2016,** *2*, 1600255.

[62] Overbury, S. H.; Kolesnikov, A. I.; Brown, G. M.; Zhang, Z.; Nair, G. S.; Sacci, R. L.; Lotfi, R.; van Duin, A. C. T.; Naguib, M. Complexity of Intercalation in MXenes: Destabilization of Urea by Two-Dimensional Titanium Carbide. *J. Am. Chem. Soc.* **2018,** *140*, 10305–10314.

[63] Mashtalir, O.; Lukatskaya, M. R.; Zhao, M.-Q.; Barsoum, M. W.; Gogotsi, Y. Amine-Assisted Delamination of Nb2C MXene for Li-Ion Energy Storage Devices. *Adv. Mater.* **2015,** *27*, 3501–3506.

[64] Alhabeb, M.; Maleski, K.; Mathis, T. S.; Sarycheva, A.; Hatter, C. B.; Uzun, S.; Levitt, A.; Gogotsi, Y. Selective Etching of Silicon from Ti3SiC2 (MAX) To Obtain 2D Titanium Carbide (MXene). *Angew. Chem. Int. Ed.* **2018,** *57*, 5444–5448.

[65] Khazaei, M.; Mishra, A.; Venkataramanan, N. S.; Singh, A. K.; Yunoki, S. Recent advances in MXenes: From fundamentals to applications. *Current Opinion in Solid State and Materials Science* **2019,** *23*, 164–178.

[66] Alhabeb, M.; Maleski, K.; Anasori, B.; Lelyukh, P.; Clark, L.; Sin, S.; Gogotsi, Y. Guidelines for Synthesis and Processing of Two-Dimensional Titanium Carbide (Ti3C2Tx MXene). *Chemistry of Materials* **2017,** *29*, 7633–7644.

[67] Zhang, J.; Kong, N.; Hegh, D.; Usman, K. A. S.; Guan, G.; Qin, S.; Jurewicz, I.; Yang, W.; Razal, J. M. Freezing Titanium Carbide Aqueous Dispersions for Ultra-long-term Storage. *ACS Applied Materials & Interfaces* **2020,** *12*, 34032–34040.

[68] Lorencova, L.; Bertok, T.; Dosekova, E.; Holazova, A.; Paprckova, D.; Vikartovska, A.; Sasinkova, V.; Filip, J.; Kasak, P.; Jerigova, M.; Velic, D.; Mahmoud, K. A.; Tkac, J. Electrochemical performance of Ti3C2Tx MXene in aqueous media: towards ultrasensitive H2O2 sensing. *Electrochim. Acta* **2017,** *235*, 471–479.

[69] Filip, J.; Zavahir, S.; Lorencova, L.; Bertok, T.; Yousaf, A. B.; Mahmoud, K. A.; Tkac, J.; Kasak, P. Tailoring electrocatalytic properties of Pt nanoparticles grown on Ti3C2Tx MXene surface. *J. Electrochem. Soc.* **2019,** *166*, H54-H62.

[70] Limbu, T. B.; Chitara, B.; Garcia Cervantes, M. Y.; Zhou, Y.; Huang, S.; Tang, Y.; Yan, F. Unravelling the Thickness Dependence and Mechanism of Surface-Enhanced Raman Scattering on Ti3C2TX MXene Nanosheets. *The Journal of Physical Chemistry C* **2020,** *124*, 17772–17782.

[71] Naguib, M.; Mashtalir, O.; Lukatskaya, M. R.; Dyatkin, B.; Zhang, C.; Presser, V.; Gogotsi, Y.; Barsoum, M. W. One-step synthesis of nanocrystalline transition metal oxides on thin sheets of disordered graphitic

carbon by oxidation of MXenes. *Chemical Communications* **2014,** *50*, 7420–7423.

[72] Lorencova, L.; Bertok, T.; Filip, J.; Jerigova, M.; Velic, D.; Kasak, P.; Mahmoud, K. A.; Tkac, J. Highly stable Ti3C2Tx (MXene)/Pt nanoparticles-modified glassy carbon electrode for H2O2 and small molecules sensing applications. *Sens. Actuat. B: Chem.* **2018,** *263*, 360–368.

[73] Lorencova, L.; Gajdosova, V.; Hroncekova, S.; Bertok, T.; Jerigova, M.; Velic, D.; Sobolciak, P.; Krupa, I.; Kasak, P.; Tkac, J. Electrochemical Investigation of Interfacial Properties of Ti3C2Tx MXene Modified by Aryldiazonium Betaine Derivatives. *Front. Chem.* **2020,** *8*, 553, DOI: 10.3389/fchem.2020.00553.

[74] Ji, J.; Zhao, L.; Shen, Y.; Liu, S.; Zhang, Y. Covalent stabilization and functionalization of MXene via silylation reactions with improved surface properties. *FlatChem* **2019,** *17*, 100128.

[75] Cao, W.-T.; Feng, W.; Jiang, Y.-Y.; Ma, C.; Zhou, Z.-F.; Ma, M.-G.; Chen, Y.; Chen, F. Two-dimensional MXene-reinforced robust surface superhydrophobicity with self-cleaning and photothermal-actuating binary effects. *Mater. Horizons* **2019,** *6*, 1057–1065.

[76] Lim, S.; Park, H.; Yang, J.; Kwak, C.; Lee, J. Stable colloidal dispersion of octylated Ti3C2-MXenes in a nonpolar solvent. *Colloids Surf., A* **2019,** *579*, 123648.

[77] Kumar, S.; Lei, Y.; Alshareef, N. H.; Quevedo-Lopez, M. A.; Salama, K. N. Biofunctionalized two-dimensional Ti3C2 MXenes for ultrasensitive detection of cancer biomarker. *Biosens. Bioelectron.* **2018,** *121*, 243–249.

[78] Bertok, T.; Lorencova, L.; Hroncekova, S.; Gajdosova, V.; Jane, E.; Hires, M.; Kasak, P.; Kaman, O.; Sokol, R.; Bella, V.; Eckstein, A. A.; Mosnacek, J.; Vikartovska, A.; Tkac, J. Advanced impedimetric biosensor configuration and assay protocol for glycoprofiling of a prostate oncomarker using Au nanoshells with a magnetic core. *Biosens. Bioelectron.* **2019,** *131*, 24–29.

[79] Bertok, T.; Dosekova, E.; Belicky, S.; Holazova, A.; Lorencova, L.; Mislovicova, D.; Paprckova, D.; Vikartovska, A.; Plicka, R.; Krejci, J.; Ilcikova, M.; Kasak, P.; Tkac, J. Mixed Zwitterion-Based Self-Assembled Monolayer Interface for Impedimetric Glycomic Analyses of Human IgG Samples in an Array Format. *Langmuir* **2016,** *32*, 7070–7078.

[80] Hetemi, D.; Noël, V.; Pinson, J. Grafting of diazonium salts on surfaces: Application to biosensors. *Biosensors* **2020,** *10*.

[81] Xu, B.; Zhi, C.; Shi, P. Latest advances in MXene biosensors. *Journal of Physics: Materials* **2020,** *3*, 031001.

[82] Kamysbayev, V.; Filatov, A. S.; Hu, H.; Rui, X.; Lagunas, F.; Wang, D.; Klie, R. F.; Talapin, D. V. Covalent surface modifications and superconductivity of two-dimensional metal carbide MXenes. *Science* **2020**, eaba8311.

[83] Liu, P.; Yao, Z.; Ng, V. M. H.; Zhou, J.; Kong, L. B.; Yue, K. Facile synthesis of ultrasmall Fe3O4 nanoparticles on MXenes for high microwave absorption performance. *Compos. Part A-Appl. Sci.* **2018,** *115*, 371–382.

[84] Rakhi, R. B.; Nayak, P.; Xia, C.; Alshareef, H. N. Novel amperometric glucose biosensor based on MXene nanocomposite. *Sci. Rep.* **2016,** *6*, 36422.

[85] Satheeshkumar, E.; Makaryan, T.; Melikyan, A.; Minassian, H.; Gogotsi, Y.; Yoshimura, M. One-step Solution Processing of Ag, Au and Pd@MXene Hybrids for SERS. *Sci. Rep.* **2016,** *6*, 32049.

[86] Jiang, Y.; Zhang, X.; Pei, L.; Yue, S.; Ma, L.; Zhou, L.; Huang, Z.; He, Y.; Gao, J. Silver nanoparticles modified two-dimensional transition metal carbides as nanocarriers to fabricate acetycholinesterase-based electrochemical biosensor. *Chem. Eng. J.* **2018,** *339*, 547–556.

[87] Song, D.; Jiang, X.; Li, Y.; Lu, X.; Luan, S.; Wang, Y.; Li, Y.; Gao, F. Metal−organic frameworks-derived MnO2/Mn3O4 microcuboids with hierarchically ordered nanosheets and Ti3C2 MXene/Au NPs composites for electrochemical pesticide detection. *J. Hazard. Mater.* **2019,** *373*, 367–376.

[88] Mohammadniaei, M.; Koyappayil, A.; Sun, Y.; Min, J.; Lee, M.-H. Gold nanoparticle/MXene for multiple and sensitive detection of oncomiRs based on synergetic signal amplification. *Biosens. Bioelectron.* **2020,** *159*, 112208.

[89] Zheng, J.; Diao, J.; Jin, Y.; Ding, A.; Wang, B.; Wu, L.; Weng, B.; Chen, J. An Inkjet Printed Ti3C2-GO Electrode for the Electrochemical Sensing of Hydrogen Peroxide. *J. Electrochem. Soc.* **2018,** *165*.

[90] Hroncekova, S.; Bertók, T.; Hires, M.; Jane, E.; Lorencova, L.; Vikartovská, A.; Tanvir, A.; Kasák, P.; Tkac, J. Ultrasensitive Ti3C2TX MXene/Chitosan Nanocomposite-Based Amperometric Biosensor for Detection of Potential Prostate Cancer Marker in Urine Samples. *Processes* **2020,** *8*, 580.

[91] Tkac, J.; Ruzgas, T. Dispersion of single walled carbon nanotubes. Comparison of different dispersing strategies for preparation of modified electrodes toward hydrogen peroxide detection. *Electrochem. Commun.* **2006,** *8*, 899–903.

[92] Tkac, J.; Whittaker, J. W.; Ruzgas, T. The use of single walled carbon nanotubes dispersed in a chitosan matrix for preparation of a galactose biosensor. *Biosens. Bioelectron.* **2007,** *22*, 1820–1824.

[93] Wang, F.; Yang, C.; Duan, C.; Xiao, D.; Tang, Y.; Zhu, J. An Organ-Like Titanium Carbide Material (MXene) with Multilayer Structure Encapsulating Hemoglobin for a Mediator-Free Biosensor. *J. Electrochem. Soc.* **2014,** *162*, B16-B21.

[94] Liu, H.; Duan, C.; Yang, C.; Shen, W.; Wang, F.; Zhu, Z. A novel nitrite biosensor based on the direct electrochemistry of hemoglobin immobilized on MXene-Ti3C2. *Sens. Actuat. B: Chem.* **2015,** *218*, 60–66.

[95] Zheng, J.; Wang, B.; Jin, Y.; Weng, B.; Chen, J. Nanostructured MXene-based biomimetic enzymes for amperometric detection of superoxide anions from HepG2 cells. *Microchim. Acta* **2019,** *186*, 95.

[96] Wang, F.; Yang, C.; Duan, M.; Tang, Y.; Zhu, J. TiO2 nanoparticle modified organ-like Ti3C2 MXene nanocomposite encapsulating hemoglobin for a mediator-free biosensor with excellent performances. *Biosens. Bioelectron.* **2015,** *74*, 1022–1028.

[97] Zhang, H.; Wang, Z.; Zhang, Q.; Wang, F.; Liu, Y. Ti3C2 MXenes nanosheets catalyzed highly efficient electrogenerated chemiluminescence biosensor for the detection of exosomes. *Biosens. Bioelectron.* **2019,** *124–125*, 184–190.

[98] Zheng, J.; Wang, B.; Ding, A.; Weng, B.; Chen, J. Synthesis of MXene/DNA/Pd/Pt nanocomposite for sensitive detection of dopamine. *J. Electroanal. Chem.* **2018,** *816*, 189–194.

[99] Zhang, Y.; Jiang, X.; Zhang, J.; Zhang, H.; Li, Y. Simultaneous voltammetric determination of acetaminophen and isoniazid using MXene modified screen-printed electrode. *Biosens. Bioelectron.* **2019,** *130*, 315–321.

[100] Xiang, H.; Lin, H.; Yu, L.; Chen, Y. Hypoxia-Irrelevant Photonic Thermodynamic Cancer Nanomedicine. *ACS Nano* **2019,** *13*, 2223–2235.

[101] Chae, A.; Jang, H.; Koh, D.-Y.; Yang, C.-M.; Kim, Y.-K. Exfoliated MXene as a mediator for efficient laser desorption/ionization mass spectrometry analysis of various analytes. *Talanta* **2020,** *209*, 120531.

[102] Jiang, Y.; Sun, J.; Cui, Y.; Liu, H.; Zhang, X.; Jiang, Y.; Nie, Z. Ti3C2 MXene as a novel substrate provides rapid differentiation and quantitation of glycan isomers with LDI-MS. *Chem. Commun.* **2019,** *55*, 10619–10622.

[103] Zamora-Gálvez, A.; Morales-Narváez, E.; Mayorga-Martinez, C. C.; Merkoçi, A. Nanomaterials connected to antibodies and molecularly imprinted polymers as bio/receptors for bio/sensor applications. *Applied Materials Today* **2017,** *9*, 387–401.

[104] Sinha, A.; Dhanjai; Mugo, S. M.; Chen, J.; Lokesh, K. S. MXene-based sensors and biosensors: Next-generation detection platforms. In *Handbook of Nanomaterials in Analytical Chemistry: Modern Trends in Analysis*, 2019, pp 361–372.

[105] Grieshaber, D.; MacKenzie, R.; Vörös, J.; Reimhult, E. Electrochemical Biosensors - Sensor Principles and Architectures. *Sensors* **2008,** *8*, 1400–1458.

[106] Jastrzębska, A. M.; Szuplewska, A.; Rozmysłowska-Wojciechowska, A.; Chudy, M.; Olszyna, A.; Birowska, M.; Popielski, M.; Majewski, J. A.; Scheibe, B.; Natu, V.; Barsoum, M. W. On tuning the cytotoxicity of Ti3C2 (MXene) flakes to cancerous and benign cells by post-delamination surface modifications. *2D Materials* **2020,** *7*.

[107] Gajdosova, V.; Lorencova, L.; Kasak, P.; Tkac, J. Electrochemical Nanobiosensors for Detection of Breast Cancer Biomarkers. *Sensors* **2020,** *20*, 4022.

[108] Siegel, R. L.; Miller, K. D.; Jemal, A. Cancer statistics, 2019. *CA Cancer J Clin* **2019,** *69*, 7–34.

[109] Atkinson, A. J., Jr.; Colburn, W. A.; DeGruttola, V. G.; DeMets, D. L.; Downing, G. J.; Hoth, D. F.; Oates, J. A.; Peck, C. C.; Schooley, R. T.; Spilker, B. A.; Woodcock, J.; Zeger, S. L. Biomarkers and surrogate endpoints: Preferred definitions and conceptual framework. *Clin. Pharmacol. Ther.* **2001,** *69*, 89–95.

[110] Tzitzikos, G.; Saridi, M.; Filippopoulou, T.; Makri, A.; Goulioti, A.; Stavropoulos, T.; Stamatiou, K. Measurement of tumor markers in chronic hemodialysis patients. *Saudi J. Kidney Dis. Transplant.* **2010,** *21*, 50–53.

[111] Núñez, C. Blood-based protein biomarkers in breast cancer. *Clin. Chim. Acta* **2019,** *490*, 113–127.

[112] Estakhri, R.; Ghahramanzade, A.; Vahedi, A.; Nourazarian, A. Serum levels of CA15–3, AFP, CA19–9 and CEA tumor markers in cancer care and treatment of patients with impaired renal function on hemodialysis. *Asian Pacific journal of cancer prevention : APJCP* **2013,** *14*, 1597–9.

[113] Gebrehiwot, A. G.; Melka, D. S.; Kassaye, Y. M.; Gemechu, T.; Lako, W.; Hinou, H.; Nishimura, S.-I. Exploring serum and immunoglobulin G N-glycome as diagnostic biomarkers for early detection of breast cancer in Ethiopian women. *BMC Cancer* **2019,** *19*, 588.

[114] Bertok, T.; Lorencova, L.; Chocholova, E.; Jane, E.; Vikartovska, A.; Kasak, P.; Tkac, J. Electrochemical Impedance Spectroscopy Based Biosensors: Mechanistic Principles, Analytical Examples and Challenges

towards Commercialization for Assays of Protein Cancer Biomarkers. *ChemElectroChem* **2019,** *6*, 989–1003.

[115] Lorencova, L.; Bertok, T.; Bertokova, A.; Gajdosova, V.; Hroncekova, S.; Vikartovska, A.; Kasak, P.; Tkac, J. Exosomes as a Source of Cancer Biomarkers: Advances in Electrochemical Biosensing of Exosomes. *ChemElectroChem* **2020,** *7*, 1956–1973.

[116] Reddy, K. K.; Bandal, H.; Satyanarayana, M.; Goud, K. Y.; Gobi, K. V.; Jayaramudu, T.; Amalraj, J.; Kim, H. Recent Trends in Electrochemical Sensors for Vital Biomedical Markers Using Hybrid Nanostructured Materials. *Adv. Sci.* **2020,** *7*, 1902980.

[117] Wang, H.; Sun, J.; Lu, L.; Yang, X.; Xia, J.; Zhang, F.; Wang, Z. Competitive electrochemical aptasensor based on a cDNA-ferrocene/MXene probe for detection of breast cancer marker Mucin1. *Anal. Chim. Acta* **2020,** *1094*, 18–25.

[118] Liu, L.; Wei, Y.; Jiao, S.; Zhu, S.; Liu, X. A novel label-free strategy for the ultrasensitive miRNA-182 detection based on MoS2/Ti3C2 nanohybrids. *Biosens. Bioelectron.* **2019,** *137*, 45–51.

[119] Duan, F.; Guo, C.; Hu, M.; Song, Y.; Wang, M.; He, L.; Zhang, Z.; Pettinari, R.; Zhou, L. Construction of the 0D/2D heterojunction of Ti3C2Tx MXene nanosheets and iron phthalocyanine quantum dots for the impedimetric aptasensing of microRNA-155. *Sens. Actuat. B: Chem.* **2020,** *310*, 127844.

[120] Xu, Q.; Xu, J.; Jia, H.; Tian, Q.; Liu, P.; Chen, S.; Cai, Y.; Lu, X.; Duan, X.; Lu, L. Hierarchical Ti3C2 MXene-derived sodium titanate nanoribbons/PEDOT for signal amplified electrochemical immunoassay of prostate specific antigen. *J. Electroanal. Chem.* **2020,** *860*, 113869.

[121] Chen, J.; Tong, P.; Huang, L.; Yu, Z.; Tang, D. Ti3C2 MXene nanosheet-based capacitance immunoassay with tyramine-enzyme repeats to detect prostate-specific antigen on interdigitated micro-comb electrode. *Electrochim. Acta* **2019,** *319*, 375–381.

[122] Liu, Y.; Zeng, H.; Chai, Y.; Yuan, R.; Liu, H. Ti3C2/BiVO4 Schottky junction as a signal indicator for ultrasensitive photoelectrochemical detection of VEGF165. *Chem. Commun.* **2019,** *55*, 13729–13732.

[123] Kumar, R.; Pal, S.; Verma, A.; Prajapati, Y. K.; Saini, J. P. Effect of silicon on sensitivity of SPR biosensor using hybrid nanostructure of black phosphorus and MXene. *Superlattices Microstruct.* **2020,** *145*, 106591.

[124] Wu, L.; You, Q.; Shan, Y.; Gan, S.; Zhao, Y.; Dai, X.; Xiang, Y. Few-layer Ti3C2Tx MXene: A promising surface plasmon resonance biosensing material to enhance the sensitivity. *Sens. Actuat. B: Chem.* **2018,** *277*, 210–215.

[125] Srivastava, A.; Verma, A.; Das, R.; Prajapati, Y. K. A theoretical approach to improve the performance of SPR biosensor using MXene and black phosphorus. *Optik* **2020,** *203*, 163430.

[126] Ding, X.; Li, C.; Wang, L.; Feng, L.; Han, D.; Wang, W. Fabrication of hierarchical g-C3N4/MXene-AgNPs nanocomposites with enhanced photocatalytic performances. *Mater. Lett.* **2019,** *247*, 174–177.

[127] Wu, Q.; Li, N.; Wang, Y.; Xu, Y.; Wu, J.; Jia, G.; Ji, F.; Fang, X.; Chen, F.; Cui, X. Ultrasensitive and Selective Determination of Carcinoembryonic Antigen Using Multifunctional Ultrathin Amino-Functionalized Ti3C2-MXene Nanosheets. *Anal. Chem.* **2020,** *92*, 3354–3360.

[128] Wang, S.; Wei, S.; Wang, S.; Zhu, X.; Lei, C.; Huang, Y.; Nie, Z.; Yao, S.

Chimeric DNA-Functionalized Titanium Carbide MXenes for Simultaneous Mapping of Dual Cancer Biomarkers in Living Cells. *Anal. Chem.* **2019,** *91*, 1651–1658.

[129] Guo, Z.; Zhu, X.; Wang, S.; Lei, C.; Huang, Y.; Nie, Z.; Yao, S. Fluorescent Ti3C2 MXene quantum dots for an alkaline phosphatase assay and embryonic stem cell identification based on the inner filter effect. *Nanoscale* **2018,** *10*, 19579–19585.

[130] Chen, F.; Lu, Q.; Zhang, Y.; Yao, S. Strand displacement dual amplification miRNAs strategy with FRET between NaYF4:Yb,Tm/Er upconversion nanoparticles and Ti3C2 nanosheets. *Sens. Actuat. B: Chem.* **2019,** *297*.

[131] Cai, G.; Yu, Z.; Tong, P.; Tang, D. Ti3C2 MXene quantum dot-encapsulated liposomes for photothermal immunoassays using a portable near-infrared imaging camera on a smartphone. *Nanoscale* **2019,** *11*, 15659–15667.

[132] Fang, D.; Zhang, S.; Dai, H.; Lin, Y. An ultrasensitive ratiometric electrochemiluminescence immunosensor combining photothermal amplification for ovarian cancer marker detection. *Biosens. Bioelectron.* **2019,** *146*.

[133] Zhang, H.; Wang, Z.; Zhang, Q.; Wang, F.; Liu, Y. Ti 3 C 2 MXenes nanosheets catalyzed highly efficient electrogenerated chemiluminescence biosensor for the detection of exosomes. *Biosens. Bioelectron.* **2019,** *124–125*, 184–190.

[134] Zhang, Q.; Wang, F.; Zhang, H.; Zhang, Y.; Liu, M.; Liu, Y. Universal Ti3C2 MXenes Based Self-Standard Ratiometric Fluorescence Resonance Energy Transfer Platform for Highly Sensitive Detection of Exosomes. *Anal. Chem.* **2018,** *90*, 12737–12744.

[135] Fang, D.; Zhao, D.; Zhang, S.; Huang, Y.; Dai, H.; Lin, Y. Black phosphorus quantum dots functionalized MXenes as the enhanced dual-mode probe for exosomes sensing. *Sens. Actuat. B: Chem.* **2020,** *305*, 127544.

[136] Mohammadniaei, M.; Nguyen, H. V.; Tieu, M. V.; Lee, M.-H. 2D Materials in Development of Electrochemical Point-of-Care Cancer Screening Devices. *Micromachines* **2019,** *10*, 662.

[137] Lin, H.; Chen, Y.; Shi, J. Insights into 2D MXenes for Versatile Biomedical Applications: Current Advances and Challenges Ahead. *Adv. Sci.* **2018,** *5*, 1800518.